W. F. Smith

Department of Meteorology
University of Wisconsin

WBG - 10

1 October 1964

STUDIES IN ATMOSPHERIC ENERGETICS

BASED ON AERO - SPACE PROBINGS

Annual Report
Contract WBG - 10

The research in this document has been sponsored by the National Weather Satellite Center, Meteorological Satellite Laboratory and the office of Meteorological Research, U. S. Department of Commerce, Weather Bureau.

ANNUAL REPORT ON RESEARCH, 1963 - 1964

GRANT WBG - 10

U.S. Department of Commerce, Weather Bureau

Submitted by:

Professor V.E. Suomi,* Department of Meteorology

Professor R.J. Parent, Department of Electrical Engineering

The University of Wisconsin, Madison, Wisconsin

Project 1: Basic Research on Physical Methods and Instrumentation for Satellite and Airborne Probings of the Atmosphere.

Project 2: Empirical and Theoretical Studies of Energy Input and Output at the Fringes of the Atmosphere.

Project 3: Empirical and Theoretical Studies of Transfer and Transformations of Radiative Energy within Atmospheric Columns.

*On leave of absence September 1, 1964 -- August 31, 1965

TABLE OF CONTENTS

1. INTRODUCTION

The research reported in this document was performed under Grant WBG-10 during the time period from 1 October, 1963 through 30 September, 1964 at the University of Wisconsin. The following personnel were engaged in the various phases of this research: Professor V. E. Suomi, Professor R. J. Parent, Dr. P. M. Kuhn, Dr. J. A. Weinman, Mr. S. K. Cox, Mr. Y. J. Lin, Mr. A. F. Hasler, Mr. R. G. Knollenberg, and Mr. P. E. Neevel.

It is our pleasant duty to acknowledge again the valuable assistance in scientific matters extended to our group by many people from outside this grant, especially the many valuable contacts with personnel of the Office of Meteorological Research and the National Weather Satellite Center, Meteorological Satellite Laboratory of the U. S. Weather Bureau.

R. J. Parent
Professor of Electrical Engineering

V. E. Suomi
Professor of Meteorology

2. PHYSICAL METHODS AND INSTRUMENTATION INVESTIGATIONS

R. J. Parent

The effort under this topic has been divided into several areas as follows:

1. Medium resolution (60-100 N. M.) operational Radiation Balance System.

An operational Radiation Balance System is currently being designed for the TOS program which will give the same type of information obtained from the University of Wisconsin Experiment flown on TIROS III, IV and VII but with higher resolution. The system under design will provide medium resolution (by definition 60-100 N. M.) by use of a number of sensors geometrically arranged to cover several tracks parallel to the orbit plane which will make measurements in a swath. Coverage probably will not be complete at the equator and there will be considerable overlap at higher latitudes.

The details of the system have been worked out and the sensor design has been essentially completed. Some hardware breadboarding has been done to verify state-of-the-art in areas where potential difficulties were apparent. As a result there are now no areas which appear to be beyond reasonable state-of-the-art solutions.

The technical and meteorological details have not yet been settled in final form, due largely to uncertainties about the spacecraft, schedules, etc. A conference has been set up to resolve these details in the very near future. We expect to get underway on a full scale program within the next month under the new W. B. Grant.

2. Cloud Reflectivity and Atmospheric Pressure Instrumentation (Weinman)

Design and fabrication of a balloon borne instrument to measure the reflectivity of clouds is nearing completion and will soon be tested.

An instrument to measure atmospheric pressure at low ambient levels has been designed and is being tested. See also 7j.

3. Data Reduction System for Radiosondes

Some preliminary work, using commercially available instruments, has been done to automatize the conversion of radiometersonde signals to digital numbers for input to a computer. The work to date has utilized tape recordings of the radiosonde receiver output and produced printouts of the data. The next step is to put the data on digital magnetic tape for direct input to a computer.

Results to date have indicated this system will increase ease, speed and accuracy of radiosonde data acquisition, particularly where further computation using the data is involved.

4. A Simple Analog to Digital Encoder (Suomi)

During the development of instrumentation for the multiple optic system of obtaining IR measurements from a cartwheel mode spin stabilized satellite a simple Analog to Digital Converter was developed. This device is able to code 0 - 1 millivolt signals into 0 - 128 or more parts. Now the limiting resolution is determined by the noise in the amplifier. The amplifier is required to raise the level of the signals from the millivolt region to the order of a few volts. In the radiosonde an 0 - 8 volt signal ordinarily exists across the thermistor. Thus it becomes possible to use the A - D converter <u>without</u> the necessity of a high gain amplifier. The temperature signals should be resolved to a few parts in 1000 or better.

The signal developed is not a steady frequency but a "chirp" or "burp" where total number of pulses is directly proportional to the EMF being measured. Thus simple ground equipment in the form of a counter can be used. The flyable equipment is also very simple, requiring only a few capacitors, resistors and possibly, one transistor.

Here we have a coder which has the potential of providing the basis for a new, rapid, economical, digital radiosonde system. Mr. Kirby Hanson has been assigned to follow up this idea in terms of its application to the radiosonde system.

3. MEASURED EFFECTIVE LONG WAVE EMISSIVITY OF CLOUDS

Peter M. Kuhn

Published in: Monthly Weather Review 91.635-640(1963)

Reprint of this research paper is attached
to this report as Appendix No. 1

4. AIRBORNE RADIOMETER MEASUREMENTS OF EFFECTS OF PARTICULATES ON TERRESTRIAL FLUX*

P. M. Kuhn[1] and V. E. Suomi[2]

[1]Office of Meteorological Research, U. S. Dept. of Commerce, Weather Bureau, University of Wisconsin, Madison, Wisconsin

[2]Dept. of Meteorology, University of Wisconsin, Madison, Wisconsin

*Accepted for publication in Journal of Applied Meteorology

AIRBORNE RADIOMETER MEASUREMENTS OF EFFECTS OF PARTICULATES ON TERRESTRIAL FLUX

Abstract

Thin layers of particulates or clouds in the high troposphere and lower stratosphere are generally not visible to an observer at the surface, even under the favorable viewing conditions at sunset. They are not easily detected by a television camera in a satellite from above. Yet these layers affect upwelling infrared flux.

A flight program employing balloon borne radiometers and a jet aircraft from which visual observations of particle layers were made was conducted to measure the attenuating effects of these layers on upwelling terrestrial flux. An estimate of the error such attenuation can cause in surface temperatures deduced from the upward flux measurement was then made. The balloon borne radiometers were launched from a desert area of California. During the ascents the presence of cirrus or particle layers could not be visually or photographically detected from the surface. They were, however, detected by the radiometer during ascent and by observers in a jet aircraft.

The observations indicated an attenuation of from .10 to .15 percent in upward infrared flux as a result of an observed particle layer beneath the higher balloon borne measurements. This attenuation could cause a 5.0°C surface temperature estimate error. Several similar observations and calculations without observers aloft show the same result.

SYMBOL TABLE

ϵ^*	Effective flux emissivity[3]
F_{E1}	Equivalent radiation flux at level 1
F_{E2}	Equivalent radiation flux at level 2
F_{BE1}	Equivalent radiation flux at level 1, assuming cloud absorptivity to be 1.0
F_{BE2}	Equivalent radiation flux at level 2, assuming cloud absorptivity to be 1.0
$F_1\uparrow$	Upward flux at level 1
$F_2\downarrow$	Downward flux at level 2
$F_{B1}\downarrow$	Downward black body flux at level 1
$F_{B2}\uparrow$	Upward black body flux at level 2
F_B	Black body flux
ϵ	Flux emissivity
w	Water vapor
c	Carbon dioxide
i, j	Indexing variables for water vapor and carbon dioxide, respectively
F_{SFC}	Surface black body flux
τ	Transmissivity
λ	Wavelength in centimeters
$F_T\uparrow$	Flux at top of atmosphere
$F_0\uparrow$	Observed flux
F_c	Calculated flux
T	Transmission (langleys/minute)

[3] All flux values are in langleys/minute.

E_{CO_2}	Emission due to carbon dioxide (langleys/minute)
T_{SFC}	Surface temperature (°C)
E_{H_2O}	Emission due to water vapor (langleys/minute)
u^*	Pressure corrected optical depth of water vapor or carbon dioxide
u	Optical depth of water vapor or carbon dioxide in precipitable centimeters of water vapor or atmospheric centimeters of carbon dioxide
$\bar{p}$	Mean pressure of atmospheric layer in millibars
p_0	Surface pressure in millibars

1. Introduction

The purpose of this study is to determine the effects of tenuous high level particulate layers on atmospheric-transmitted upwelling infrared flux. In a very dry atmosphere the transmitted flux is proportional to flux through the atmospheric window. A measure of these effects provides an estimate of errors in surface temperatures deduced from upward infrared fluxes. The effects of stratified particulate layers on atmospheric radiation have been discussed in the literature. See, for example, Deirmendjian (1960). There are, however, few simultaneous radiation and visual observations through these layers.

Conclusions drawn from this study can apply generally to the TIROS series meteorological satellite 8.0 to 12.0 micron sensor flux observations. The Nimbus meteorological satellite has a sensor in the 3.5 to 4.15 micron band. A dust particle layer would presumably have the greatest effect on the 3.5 to 4.15 micron channel measurements while ice particles would most affect the 8.0 to 12.0 micron channel measurements. This follows from considerations of the sizes of dust and ice particles. At high altitudes the former seldom have diameters over 4.0 microns while the latter generally exceed 10 microns in diameter.

Two cases of a radiometersonde ascent (Suomi and Kuhn, 1958) through the atmosphere with concurrent visual observations from a jet aircraft were made over a desert area of California in February, 1964. In a very dry atmosphere the broad response radiometersonde observations

can be used to estimate the surface temperature. Using this radiometer to simulate a satellite "window" sensor our results can show the magnitude of the attenuation of radiation by a thin high particle layer and the error in surface temperature deduced from such measurements. These errors could similarly occur in the satellite sensors. The question of erroneous surface temperature deductions from satellite sensor observations have been considered by Nordberg, et al (1962), Nordberg and Bandeen (1963), and Möller (1963). These observations provide a case study for such considerations.

2. Procedure for Observations

The radiometersonde used in these tests measures the upward and downward flux over the entire range of the infrared spectrum and overall solid angles. The soundings were made long enough after sundown to eliminate the effects of solar radiation.

A radiometer, measuring separately the upward and downward flux at a given level, integrates the emission and transmission of each of the absorbing atmospheric gases below (or above) itself. Here we are concerned only with the upward flux. In view of the uniformity of the distribution of carbon dioxide with height and of the small contribution of ozone to the radiant flux, we can isolate the water vapor emission and transmission for our broad response, low resolution radiometer. Solid geometry shows that 90 percent of the upwelling radiation reaching the

detector surface comes from an area whose radius is about 50 kilometers when the balloon is 10 kilometers high. A radiometer ascent over a homogeneous desert region extending at least twenty to thirty kilometers in all directions from the sub-balloon point, with dry air aloft, further isolates the overall atmospheric transmission measured by the radiometersonde. This is accomplished by eliminating most of the complex water vapor emission. In effect, we can simulate a low resolution, "window" response satellite sensor with the radiometersonde.

3. Flux Emissivities of Thin Cloud Layers

The radiative emission of water vapor and carbon dioxide must be removed from the balloon radiometer measurements. We are then left with energy transmitted through the atmosphere in all regions where water vapor does not absorb.

Flux emissivity may be defined as the ratio of energy actually emitted by an individual layer to what it would emit as a black body. The effective flux emissivity of a cloud (Kuhn, 1963) is the ratio of the difference in equivalent radiation at the top and base of the cloud to that equivalent radiation difference at the top and base of the same cloud considering it spectrally "black." This is equal to the ratio of the total radiation of a black surfaced slab with different top and bottom temperatures. The equation defining effective long wave flux emissivity is

$$\epsilon^* = (F_{E1} - F_{E2})/(F_{BE1} - F_{BE2}) \qquad (1)$$

The equivalent radiation is one-half the sum of the upward and downward fluxes illuminating an infinitely thin layer in the atmosphere. ϵ^* is also equal to the sum of the cloud absorptivity and reflectivity and is also equal to one minus cloud transmissivity. Fig. 1 illustrates the radiative transfers involved in equation (1). The effective flux emissivity of a cloud is in effect its blackness or its gray body emissivity or absorptivity.

The definition of the effective flux emissivity or blackness of a cloud is valid for an isothermal cloud since equivalent radiation is made up of two terms, only one of which is black body radiant energy at the ambient temperature. Thus isothermal conditions, a decrease in temperature, or, for that matter, an inversion of the ambient temperature will not invalidate the definition of effective flux emissivity.

If the atmosphere were perfectly cloudless, as we will first assume, we would expect the flux emissivity of atmospheric layers of equal thickness to generally decrease with height in a smooth manner. Exceptions occur where there are discontinuities in any absorbing media. Any sharp departures from the smooth profile could be attributed to cloud or particulate layers.

4. Surface Temperature Estimates and Calculations

Transfer theory gives the upward flux $F\uparrow$, at any level in the atmosphere. In finite difference notation by isothermal emissivities,

we have[4]

$$F\uparrow = \sum_{i=1}^{n} F_{B_{i-\frac{1}{2}}} \Delta\epsilon(w)_i + \sum_{j=1}^{n} F_{B_{j-\frac{1}{2}}} \Delta\epsilon(c)_i \qquad (2)$$

$$= (1.0 - \sum_{i=1}^{n} \Delta\epsilon(w)_i - \sum_{j=1}^{n} \Delta\epsilon(c)_i + \sum_{i=1}^{n}\sum_{j=1}^{n} \Delta\epsilon(w)_i \Delta\epsilon(c)_i) F_{sfc}\uparrow$$

In equation (2) above, only water vapor and carbon dioxide are considered. Yamamoto and Sasamori's (1958) values of carbon dioxide absorptivity were used. The transmission term, third on the right in equation (2), is merely an expansion of the appropriate expression for transmissivity by water vapor and carbon dioxide.

$$\tau(w + c) = \tau(w)\tau(c) \qquad (3)$$

The overlap effect of the transmissivities of water vapor and carbon dioxide which erroneously increases the flux is offset in the calculations by dropping the double summation term in equation (2).

Cloud and boundary conditions can be included in flux calculations by introducing the effective flux emissivity, ϵ^*, of a cloud or particle layer in equation (2). This expansion does not require that the cloud be black. Equation (2) then becomes,

---

[4] Equation (2) is equivalent to the following form of the transfer equation summed with respect to temperature

$$F\uparrow = -\sum_{0}^{\infty} F_B\uparrow \Delta\lambda + \sum_{0}^{\infty} \sum_{i=1}^{n} \uparrow_{i-\frac{1}{2}} \Delta F_{B_i} \Delta\lambda$$

Calculations by this form agree with similar calculations by equation (2).

$$F_2\uparrow = \sum_{i=1}^{n} F_{B_{i-\frac{1}{2}}} \Delta\epsilon(w)_i + \sum_{j=1}^{n} F_{B_{j-\frac{1}{2}}} \Delta\epsilon(c)_j$$

$$+ (1.0 - \sum \Delta\epsilon(w)_i - \sum \Delta\epsilon(c)_j - \sum_{i=1}^{n}\sum_{j=1}^{n} \Delta\epsilon(w)_i \Delta\epsilon(c)_j)$$

$$\times (\epsilon^* F_{B2}\uparrow + (1.0 - \epsilon^*) F_1\uparrow) \qquad (4)$$

$F_1\uparrow$ is the upward flux at layer base and F_{B2} is the upward black body flux radiating at the temperature of the top of the layer (Fig. 2).

The data obtained for this study were measured in a very dry atmosphere under subsiding conditions. There was no instrument indication of moisture during the radiometersonde ascents. The humidity element shunt resistor in the radiosonde was removed. In spite of this, no moisture signal appeared at any time during the two ascents. In order to account for any water vapor beyond the detectability limit for the humidity element, an optical mass of 300 microns was assumed.

In the calculations we start with the observed upward flux at the top of the ascent and calculate the flux at this level by introducing temperature and humidity from the same radiometer sounding. A departure in calculated and observed upward flux at the top of the ascent can be an indicator of a cloud layer since cloud effects are not used in calculations in the first instance. The aircraft observations defined the vertical position and thickness of these layers giving verification of their location. A satellite flux observation with thin clouds or particulates

intervening would suffer attenuation. The satellite estimate of the surface temperature would be too low unless appropriate cloud attenuation were introduced to make the calculation and observation agree. In this experiment we will simulate a satellite observation with radiometersonde observations and a flux calculation.

The flux calculations require the temperature, pressure, and humidity data. The observations from the radiometersonde were obtained on the same balloon. The calculations and observations can be made to agree either by the introduction of a cloud or by changing the surface temperature, T_0.

5. Surface Temperature Estimates

Two radiometersonde ascents were made after sunset on 20 February 1964. The first launch was at 1732 LST and the second at 2300 LST. Observations from the surface at both launch times indicated a clear and cloudless sky. Half-hourly reports noted visibility in the horizontal in excess of 20 miles for several hours preceding and following the balloon ascents.

A Canadian jet aircraft, RCAF 100, with pilot and observer, operated to 43000 feet throughout the balloon ascent area. The aircraft flight, in addition to furnishing continuous visual observations for this study, carried a NASA Nimbus calibration experiment aloft. The aircraft was

airborne from Edwards Air Force Base at 1800 hours LST and remained aloft for three and one-half hours.

True surface temperature measurements were made in several places across Rosamond Dry Lake and the arid region to the ~~north~~ south and ~~west~~ east of Edwards, California. Measurements were made to a distance of thirty miles to the southeast of Edwards Air Force Base. This approximated the balloon flight trajectory. The measurements were made with a number of thermistors and thermocouples attached and contiguous with the actual surfaces. Thermistors and thermocouples were gold-coated. Surface temperature measurements were also made with downward facing radiometers one meter above the surface. Direct radiometer observation just above the surface when compared with the thermistor and thermocouple sensors at the surface indicated the emissivity of the surface was approximately 0.95.

The first of the two radiometersonde ascents disclosed a continuous cloud or haze layer from 35,000 to 43,000 feet above mean sea level. This may be seen in Fig. 3 in the sharpest slope change in the equivalent radiation profile obtained directly from the original observations. It was immediately evident from a discontinuity in the original radiation temperature recorded. This technique for determining cloud layers with the radiometersonde has been recently reported (Kuhn, 1963).

After the balloon and aircraft ascents, the jet aircraft observer, Flight Lieutenant John Watson, RCAF, gave the following documented report:

The aircraft departed Edwards Air Force Base at 0200 GMT 21 February 1964. Crew members included Flight Lieutenants John Watson and Gordon A. Brown, of the Royal Canadian Air Force. The weather forecast received prior to flight was "Clear, visibility 12 miles 40,000 feet winds 280°/12 knots." A standard jet departure was accomplished and the aircraft leveled at 30,000 feet. A very slight haze condition was encountered at 35,000 feet and seemed to persist to 40,000. It was at this altitude that a layer was observed at approximately 43,000 feet that seemed thicker and more definite than at the lower levels. This observation was made looking into a very light western sky as the sun had just set minutes before. This haze layer persisted throughout the flight until darkness set in at approximately 0330 GMT.

Equation (1) was used to obtain an effective emissivity for overlapping 50 millibar layers for both flights. Apparent lower dust haze during the first flight at 750 and 320 millibars accounts for a slight increase in the effective emissivity over adjacent levels. However, the peak for the layer centered at 200 millibars measured 0.11 (Fig. 4). The arrows on each side of the plotted point at 200 millibars in Fig. 4 indicate two standard errors in the observations.

Fig. 5 gives the results of the balloon-borne radiometer measurements of the radiation and calculations of radiation from the temperature, pressure and humidity data for this 1732 LST ascent.

Fig. 5(A) shows the observed flux, F_0, at the top of the flight and also the observed average true surface temperature over the ascent area. It also shows the radiometer observed cloud layer and its emissivity. The average true surface or interface temperature measured at thirteen locations over Rosamond Dry Lake by Prof. William C. Marlatt, Colorado State University, Fort Collins, Colo., employing the Barnes Engineering Co., PRT-4 Radiometer was 6.8°C. These observations

were made between 1655 and 1800 LST. During this period the wind averaged 11.0 miles per hour from the east. This would not allow much of a surface inversion. For this same period the shelter temperature at the air base averaged 12.2°C. A radiometersonde positioned 1.0 meters above the ground and carried to seven locations south and east of Edwards Air Force Base averaged 10.9°C between 1700 and 1800 hours LST.

Fig. 5(B) gives the results of a transfer theory (Equation 4) calculation of the upward flux, F_c, at the top of the flight using the average observed true surface temperature, T_{sfc} of 8.7°C and the air temperature sounding. No cloud was introduced into this calculation. The resulting calculated flux, F_c, .443 ly/min is .041 ly/min larger than the observed flux from Fig. 5(A). Over one hundred similar soundings under assumed cloudless conditions but without observers aloft, result in calculated fluxes averaging 12% larger than concurrent radiometer observations.

Fig. 5(C) demonstrates the change in the magnitude of the upward flux calculated after the introduction of the cloud or particle layer with an effective emissivity of 0.11. This second transfer theory calculation of the upward flux in the presence of a cloud again used the observed surface temperature, 8.7°C. In this case, the calculated upward flux agreed with the observed upward flux and verifies the validity of the calculations.

Fig. 5(D) demonstrates that the calculated upward flux can be made to agree with the observed upward flux by a change in surface temperature assuming no clouds to be present. This is the case in point as agreement

between observed and calculated upward flux is accomplished by reducing the surface temperature for the calculation from 8.7 to 3.0°C. This could be interpreted as a 5.7°C error in the surface temperature if one had only a satellite upward flux or intensity measurement and no information on the presence of an intervening thin cloud layer below and in the satellite radiometer field of view.

The second radiometersonde ascent at 2300 LST disclosed only remnants of the thin cloud that was present during the earlier ascent. There was just a weak indication of a very thin or tenuous layer at 250 millibars. The observed and calculated upward flux from the same flight agreed within .01 ly/min. The observed flux at the top of the ascent was .410 ly/min, somewhat larger than on the earlier ascent in spite of a drop in the flight area averaged true surface temperature to 4.1°C from 8.7°C. The calculated flux at burst point, 28 millibars, was .420 ly/min. The true surface or interface temperature was obtained for the second ascent between 2300 and 2400 LST. It was measured with a downward facing radiometer to the southeast of Edwards Air Force Base and at the radiosonde release area. There appeared to be a variation between the Edwards shelter temperature and the radiometric determined temperatures.

6. Effects of Observational and Calculation Errors

If we assume an error of .05 in the observed flux emissivity, ϵ^*, of a cloud layer and apply this error to reduce the measured emissivity of the cloud, a 3.2°C error in the surface temperature would remain. This follows from a consideration of the analysis in Fig. 5.

The principal sources of error in the calculations of upward flux and deduced surface temperatures are incorrect surface temperatures and incorrect humidities. If the measured surface temperature used in the calculations in equation (4) were not exactly representative of the integrated surface temperature, the calculated flux for the top of the ascent would be in error accordingly. Too low a surface temperature would lead to an even larger error in the surface temperature calculation. If the surface temperature measurement were 3.0°C too high the calculated upward flux would exceed the observed by .035 langleys/minute and the corresponding surface temperature estimate would still be 2.7°C too low.

Assuming that the "dry" atmosphere actually contained 300 microns of water vapor below the radiometersonde the upward flux calculated by equation (4) including the water vapor emission and transmission was .432 langleys per minute at the top of the ascent. The pressure correction for the optical mass of the water vapor was the same as that used for carbon dioxide. The corrected optical depth is given by $u^* = u(\bar{p}/p_0)^{0.85} + 0.03(p_s/\bar{p})$ through 100 mb. Above 100 mb we used

the relationship: $u^* = u(-0.006\bar{p} + 1.0)$. The water vapor absorptivities are due to Kuhn (1963). The humidity and surface temperature errors apparently cannot account for the attenuation in upward flux that we suggest is due to an ice or dust particle layer.

7. Conclusions

A quantitative evaluation of the effects of a thin cloud layer, undetectable from above or below, on a measurement of outgoing flux and deduced surface temperature has been discussed. The effects were determined from simultaneous observations and calculations of the upward flux at the top of balloon ascents.

Observers in a jet aircraft at the level of the layer and along the balloon trajectory confirmed its presence just minutes before the balloon-borne radiometer observations responded to its presence.

Most of our radiometer ascents and all of those by Gergen (1958) into cirriform and middle altitude clouds show an increase in the equivalent radiation (Fig. 3). This phenomenon serves as an excellent boundary for the cloud base and is used in an objective computer search technique to determine the cloud or particle layer base.

Transfer calculations of the upward flux were varied by introducing a cloud and by changing the surface temperature. Both the introduction of the cloud and the changing of the surface temperature were affected to make the calculation agree with the observation. As a result errors as high as 5.7°C appear possible when undetected thin cloud or particle layers are present.

The relatively drastic reduction in upward terrestrial flux in the case of a cirrus overcast, at night, for example, makes it doubtful that low values of flux would be mistaken to mean low surface temperatures. However, the problem in surface temperature estimation occurs when high attenuating layers are present that are not detectable by television or from the surface. In these cases the surface temperature error can be quite subtle. Wark, et al (1962) has stated that the hazards in estimating surface temperatures from satellites are many and have no exact solution from satellite measurements alone. It is felt that for some time airborne radiometric observations could augment satellite flux observations until a radiation climatology has been acquired.

REFERENCES

Bushnell, R. H. and V. E. Suomi, 1961: Experimental flight verification of the economical net radiometer. J. geophys. Res., 66, 2843-2848.

Deirmendjian, D., 1960: Atmospheric extinction of infrared radiation. Quart. J. R. meteor. Soc., 86, 371-381.

Gergen, J. L., 1958: Blackness of clouds as determined from radiation measurements. Tech. Report, Nonr-710(22) School of Physics, Univ. of Minnesota.

Kuhn, P. M., 1963: Measured effective long wave emissivity of clouds. Mo. wea. Rev., 91, 635-640.

Nordberg, W., et al., 1962: Preliminary results of radiation measurements from the TIROS III meteorological satellite. J. atmos. Sci., 19, 29-30.

Nordberg, W. and W. R. Bandeen, 1963: Reply, Desert soil temperature and infrared radiation received by TIROS III. J. atmos. Sci., 20, 175-176.

Suomi, V. E. and P. M. Kuhn, 1958: An economical net radiometer. TELLUS, 10, 160-163.

Wark, D. Q., et al., 1962: Methods of estimating infrared flux and surface temperatures from meteorological satellites. J. atmos. Sci., 19, 369-384.

FIGURE LEGEND

Fig. 1. Radiative transfers defining the effective flux emissivity of an attenuating layer between levels 1 and 2.

Fig. 2. Vertical components of the radiative transfers from the surface, through an attenuating layer, to the top of the ascent.

Fig. 3. Vertical profile of the equivalent flux (open circles) and air temperatures (closed circles) for 1732 LST 20 February 1964.

Fig. 4. Vertical profile of effective flux emissivity ϵ^*, defined in equation (1), for 1732 LST 20 February 1964.

Fig. 5. Vertical profile of the equivalent flux (open circles) and air temperature (closed circles) for 2300 LST 20 February 1964.

Fig. 6. Vertical profile of effective flux emissivity ϵ^*, defined in equation (1), for 2300 LST 20 February 1964.

Fig. 7. Radiometersonde ascent, 1732 LST 20 February 1964. (A) Observed upward flux (langleys/minute) at the top of the ascent and the observed surface temperature. (B) Computed upward flux, employing observed surface temperature, assuming no intervening attenuating material other than carbon dioxide. (C) Computed upward flux, employing observed surface temperature, assuming an intervening particle layer with an effective flux emissivity of .11. (D) Computed upward flux assuming no intervening attenuating material other than carbon dioxide. This flux was calculated to be equal to the observed flux in (A) by depressing surface temperature from 8.7°C to 3.0°C.

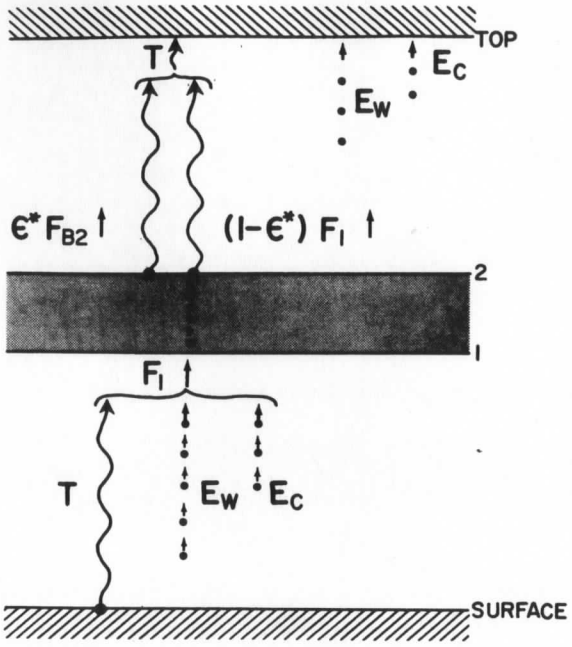
TOP
T
E_C
E_W
$\epsilon^* F_{B2}$
$(1-\epsilon^*) F_1$
2
1
F_1
T
E_W
E_C
SURFACE

Fig. 1.

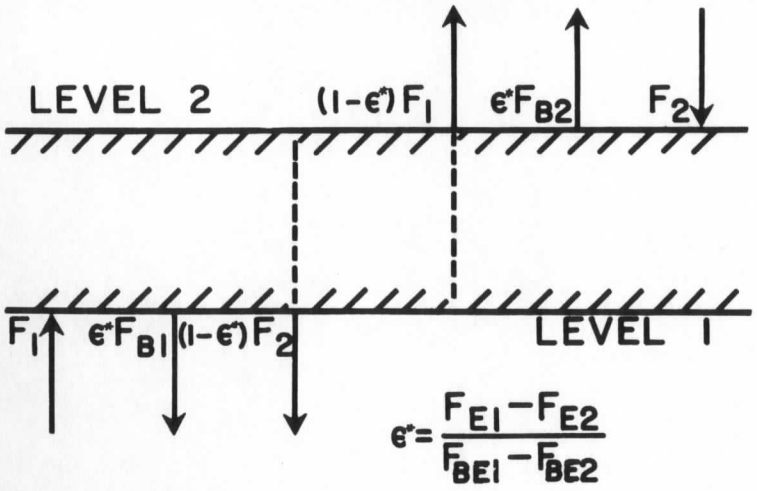
LEVEL 2
$(1-\epsilon^*) F_1$
$\epsilon^* F_{B2}$
F_2
F_1
$\epsilon^* F_{B1}$
$(1-\epsilon^*) F_2$
LEVEL 1
$\epsilon^* = \frac{F_{E1} - F_{E2}}{F_{BE1} - F_{BE2}}$

Fig. 2.

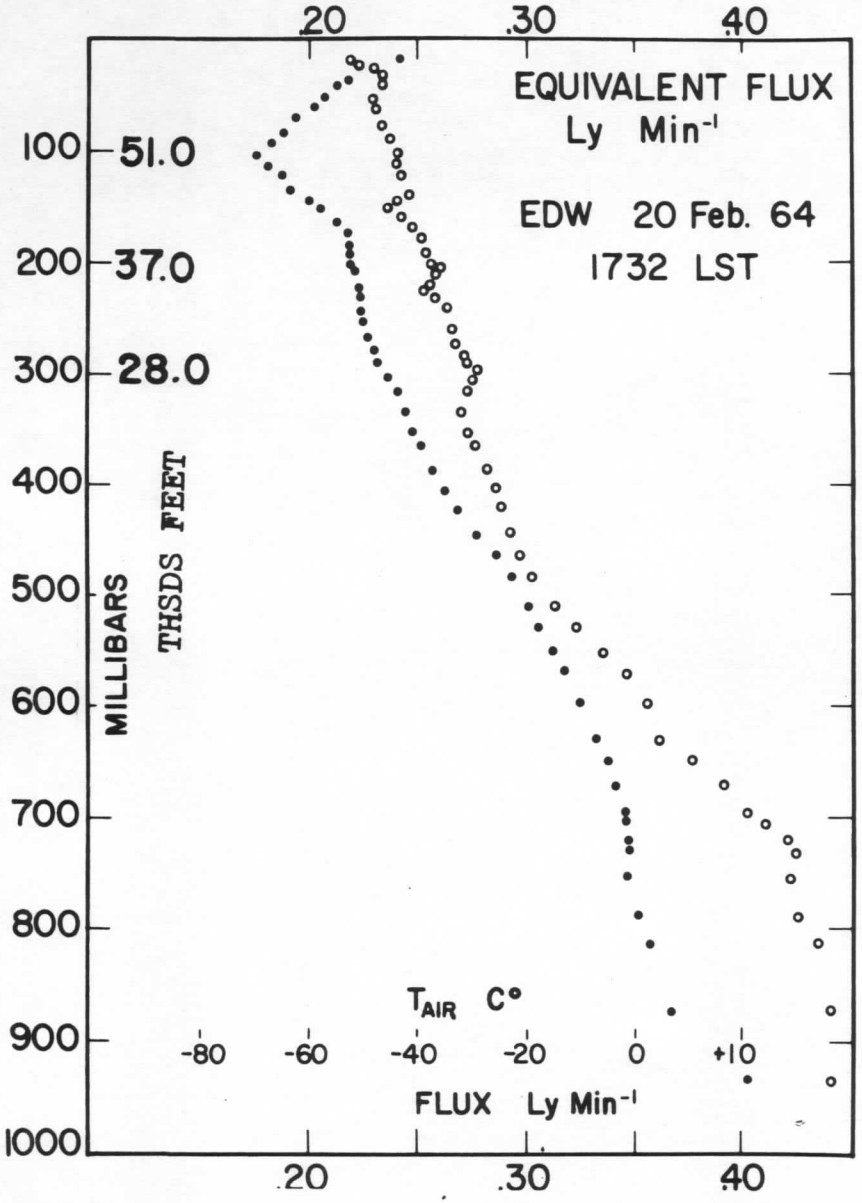
EQUIVALENT FLUX
Ly Min⁻¹
EDW 20 Feb. 64
1732 LST
MILLIBARS
THSDS FEET
51.0
37.0
28.0
100
200
300
400
500
600
700
800
900
1000
.20
.30
.40
T AIR C°
-80
-60
-40
-20
0
+10
FLUX Ly Min⁻¹

Fig. 3.

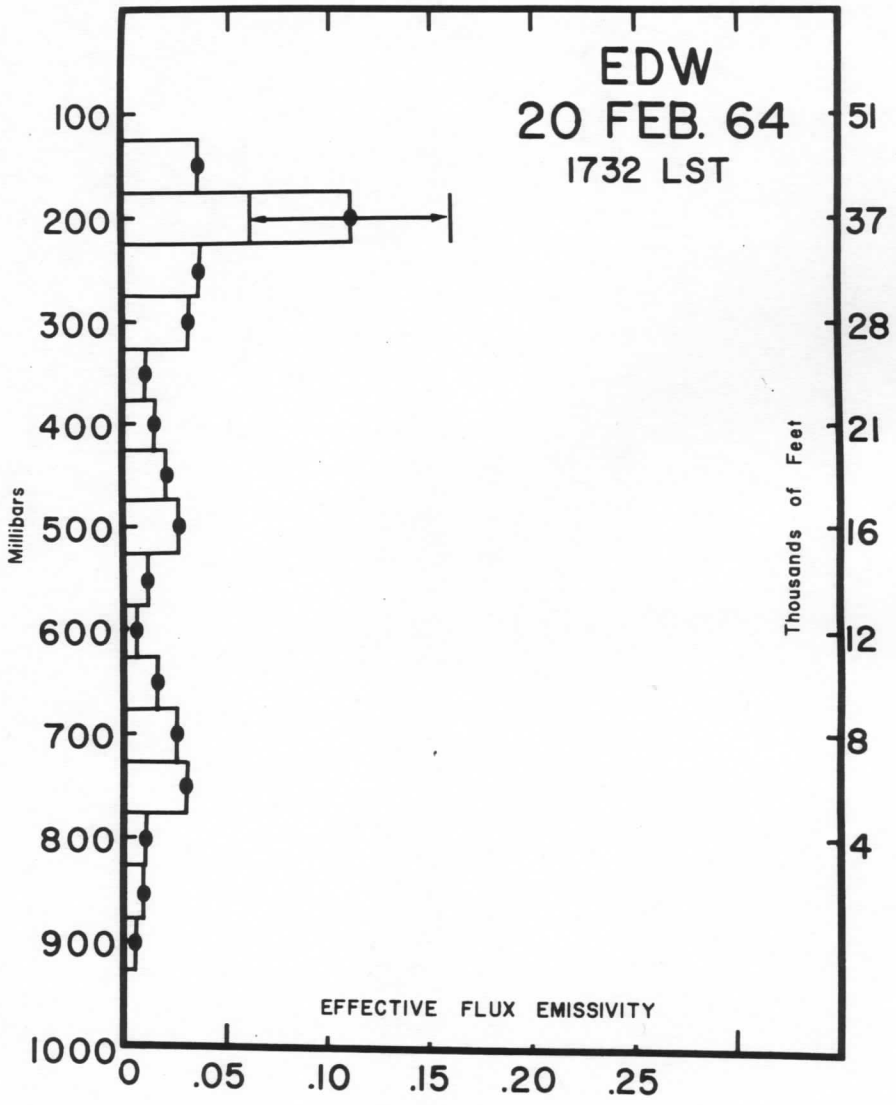
EDW
20 FEB. 64
1732 LST
Millibars
Thousands of Feet
100
200
300
400
500
600
700
800
900
1000
51
37
28
21
16
12
8
4
EFFECTIVE FLUX EMISSIVITY
0
.05
.10
.15
.20
.25

Fig. 4.

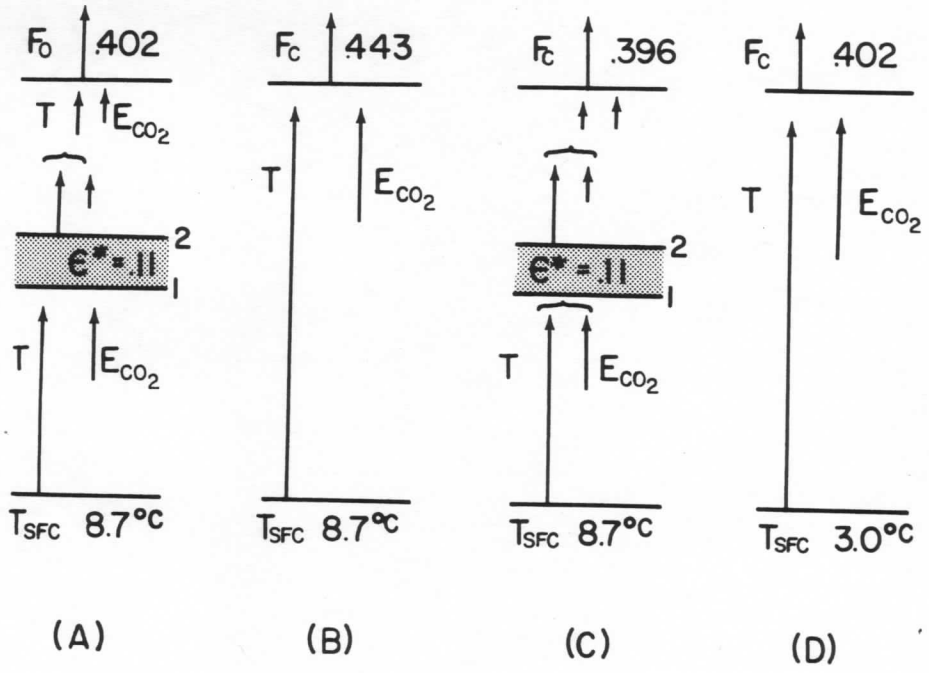
F0 .402
T
ECO2
ε* = .11
2
1
T
ECO2
TSFC 8.7°C
(A)
FC .443
T
ECO2
TSFC 8.7°C
(B)
FC .396
ε* = .11
2
1
T
ECO2
TSFC 8.7°C
(C)
FC .402
T
ECO2
TSFC 3.0°C
(D)

Fig. 5.

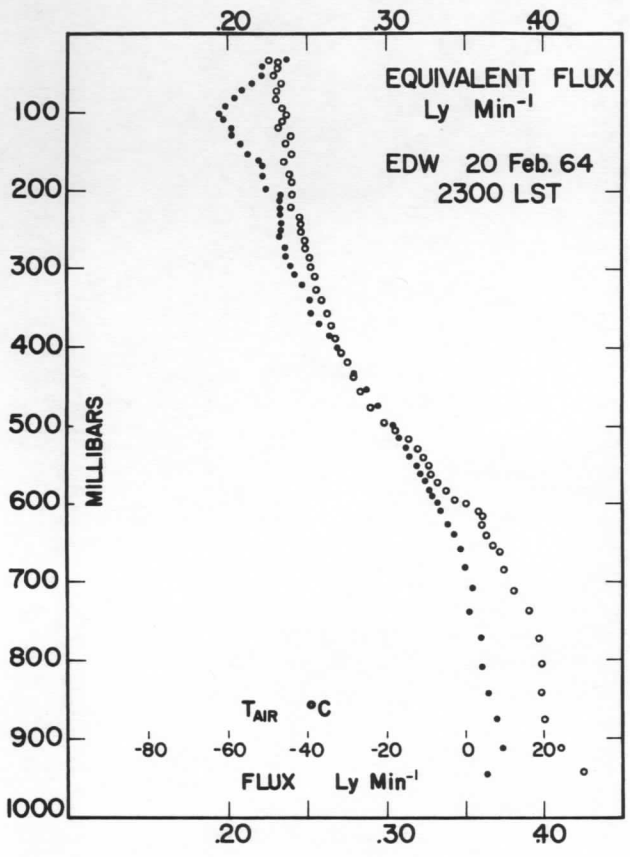
.20
.30
.40
EQUIVALENT FLUX
Ly Min⁻¹
EDW 20 Feb. 64
2300 LST
100
200
300
400
500
600
700
800
900
1000
MILLIBARS
T AIR °C
-80
-60
-40
-20
0
20°
FLUX Ly Min⁻¹
.20
.30
.40

Fig. 6.

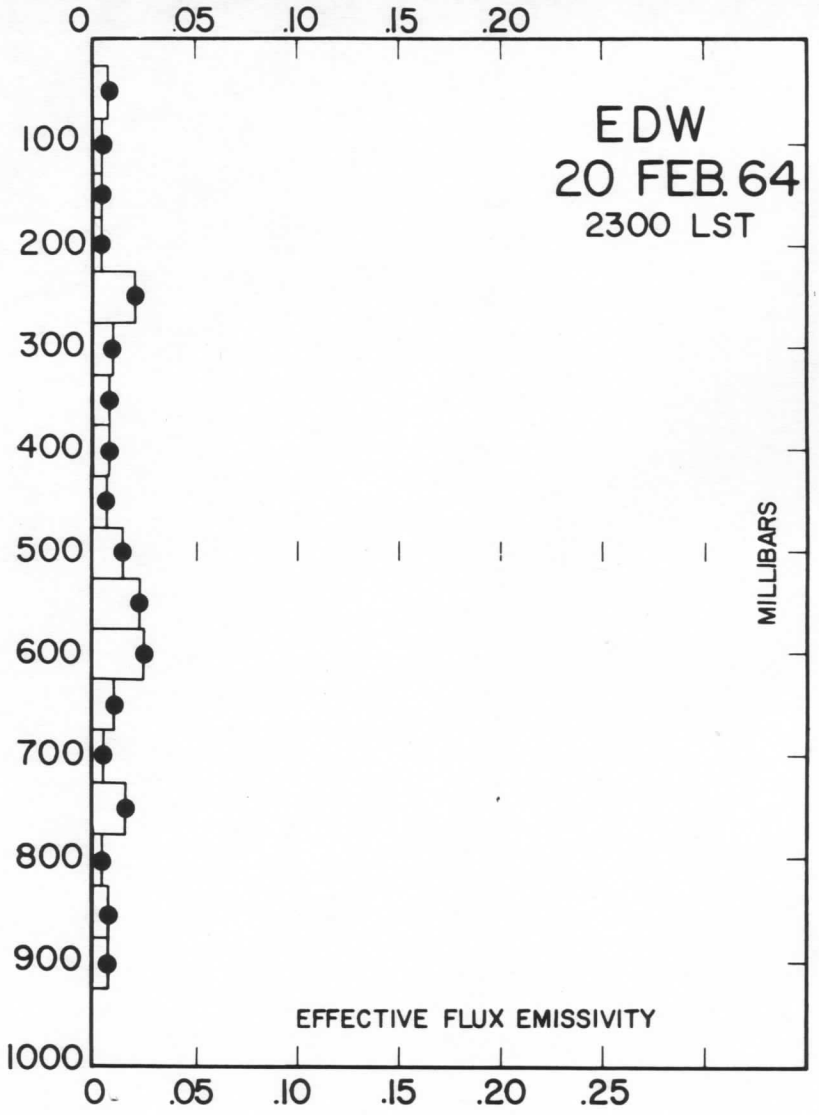
0
.05
.10
.15
.20
EDW
20 FEB. 64
2300 LST
100
200
300
400
500
600
700
800
900
1000
MILLIBARS
EFFECTIVE FLUX EMISSIVITY
0
.05
.10
.15
.20
.25

Fig. 7.

5. FEASIBILITY OF DAYTIME RADIOMETERSONDE MEASUREMENTS

Stephen K. Cox

Approved Thesis for M.S. in Meteorology

(to be published)

ABSTRACT

The feasibility of using a net radiometersonde to measure the daytime infrared and downward short-wave radiation in the absence of clouds and for sun elevation angles greater than fifty degrees is established. Results show that under cloudless conditions the standard error for the downward short-wave measurement is .101 langley/minute and for daytime infrared measurements if .061 langley/minute. The measurement of the upward short-wave flux is unsatisfactory. Under cloudy conditions the instrument performance is poor. An additional lateral conduction term is necessary in the radiometer energy balance equation because of the high temperature the radiometer attains. Three daytime radiometer flights are presented. The daytime infrared profiles are similar to nocturnal infrared measurements.

LIST OF SYMBOLS

B	= Short notation for black body function T^4, i.e. $B_t = T_t$.
C_i	= $a_i/(1-r_i(1-a_i))$, short notation for a common constant term that describes the infrared properties of the instrument.
C_s	= $a_s/(1-r(1-a_s))$, short notation for a common constant term that describes the solar properties of the instrument.
$I(\theta)$	= Short-wave radiation intensity as a function of incidence angle, θ.
$K_i(T)$, $i=1,2,3$	= Conduction constants which are a function of the mean temperature between the two surfaces involved.
L_t, L_b	= Conduction losses from radiometer sensor surface.
R_{id}, R_{iu}	= Infrared radiation flux density downward and upward, respectively.
R_{sd}, R_{su}	= Short-wave radiation flux density downward and upward, respectively.
T_t, T_b, T_a	= Absolute temperature of the top radiation surface, the bottom radiation surface, and air, respectively.
a_i, a_s	= Absorptivity of infrared and solar radiation, respectively, of the radiative surface.

List of Symbols continued

r_i, r_s = Reflectivity of infrared and solar radiation, respectively, by the polyethylene films.

ε_i, ε_s = Emissivity of the polyethylene for infrared and solar radiation, respectively.

τ_i, τ_s = Transmissivity of polyethylene for infrared and solar radiation, respectively.

$\tau_s(\theta)$ = Transmissivity of polyethylene as a function of incidence angle, θ, for solar radiation.

Subscripts:

d, u indicate downward and upward radiation currents, respectively.

i, s indicate infrared and short wave, respectively.

t, b indicate top and bottom radiation surfaces, respectively.

b, w indicate black and white 'paints', respectively.

I. INTRODUCTION

Two radiometersondes with different spectral characteristics can be used to measure separately the infrared and short-wave radiation. Because of the fortunate spectral characteristics of white paints, a white radiometer essentially measures the infrared component, and a black radiometer measures both the infrared and short-wave energy. The short-wave energy is the difference between the black and the white radiometer measurements.

The measurement of infrared radiation during the day using two radiometers was discussed by Tanner, Businger, and Kuhn (1960). Schoffer and Kuhn (1961) compared results of solar energy measurements by a black and white radiometer system with those from silicon cells and an Eppley pyrheliometer.

The purpose of this study was to determine the feasibility of using this radiometersonde to separately deduce the long-wave and short-wave radiation profiles throughout the atmosphere during daylight hours.

II. THEORY

2.1 Conduction and Convection

The balloon version of the radiometersonde was originally designed for nocturnal infrared measurements where sensor temperatures and temperature gradients are not as extreme as in daytime ascents. In daytime ascents it is common to encounter air temperatures at the tropopause of 203 degrees Absolute while the top black radiometer surface maintains a temperature in excess of 353 degrees Absolute. This large temperature gradient magnifies the importance of an accurate conduction term in the evaluation of the radiometersonde data.

The basic theory of the radiometersonde was presented by Suomi, Staley, and Kuhn (1958). This same theory applies to the daytime application of the radiometersonde with one exception. In the nighttime use of the instrument, the top and the bottom sensor surfaces are lower and higher, respectively, than air temperature. In this case, the top sensor gains energy, and the bottom sensor loses energy by lateral conduction. Since the top and bottom sensors are coupled by vertical conduction, the net energy gain or loss of the instrument by lateral conduction would be very small. This cancellation effect is the justification for the omission of such a lateral conduction term in the nighttime case. The lateral conduction terms are quite small at night and even without the previously mentioned cancellation effect, their contribution is usually essentially negligible. Figure 1 shows the magnitude of the lateral conduction term in a typical

nocturnal ascent.

In the daytime application of the radiometersonde, all four sensor surface temperatures exceed air temperature. With the symmetry of the top and bottom surface temperatures about air temperature removed, the cancellation effect of the lateral conduction terms no longer exists.

Figure 2 illustrates the magnitude of this lateral conduction term as a function of temperature difference between air and the top black radiometer surface in a typical daytime flight.

Applying the method of De Graaf, et. al., (1953) to the geometry of the instrument shows that all convective heat transfer is suppressed at the high temperature gradients encountered in daytime ascents.

2.2 Polyethylene Reflectivity

For incident short-wave radiation emanating from above a solar altitude of 45 degrees relative to the radiometer face, the polyethylene reflectivity is not an important function of incidence angle. However, below an altitude of 45 degrees, the polyethylene reflectivity becomes a rapidly varying function of incidence angle. Figure 3 shows the short-wave reflectivity of .01 inch polyethylene as a function of solar elevation angle given by Tanner and Kuhn (1962).

2.3 Absorptivity of the White Sensor

In the use of the black and white radiometers, the constant least reliably known is the absorptivity of the white surface in

the short-wave region of the spectrum. The short-wave absorptivity of the white surface, a_{sw}, may vary with method of application, humidity conditions, texture of the surface, and the time between coating and use. This inconsistency was met with an in-flight calibration procedure.

2.4 Equations

The energy balance equations of the radiometer surface enable one to solve separately for both the infrared and the short-wave radiation values. There are two equations with two unknowns. One equation is from the black radiometer absorbing over eighty per cent of both the infrared and short-wave radiation incident upon it and the other from the white radiometer absorbing only twenty percent of the incident short-wave energy but eighty per cent of the infrared energy. These two equations allow one to solve for the two unknown quantities -- the infrared and the short-wave radiation.

Assuming no convective transfer, the energy balance equation for the top surface of the black radiometer is given by equation (1).

$$C_{sb}\left[\frac{\sum_{\theta=0}^{\pi/2} I(\theta)\tau_s(\theta)}{\sum_{\theta=0}^{\pi/2} I(\theta)}\right] R_{sd} + C_{ib}\,\tau_i\,R_{id} = C_{ib}(1-r_i)B_{tb} - C_{ib}\epsilon_i B_{ptb} + L_{tb} \qquad (1)$$

where

$$L_{tb} = K_1(\bar{T})\left[T_{tb} - T_a\right] + K_2(\bar{T})\left[T_{tb} - T_a\right] + K_3(\bar{T})\left[T_{tb} - T_{bb}\right] \qquad (2)$$

The energy balance equation for the top surface of the white radiometer is

$$C_{sw}\left|\frac{\sum_{\theta=0}^{\pi/2} I(\theta)\,\tau_s(\theta)}{\sum_{\theta=0}^{\pi/2} I(\theta)}\right| R_{sd} + C_{iw}\,\tau_i\,R_{id} = C_{iw}(1-r_i)B_{tw} - C_{iw}\,\epsilon_i\,B_{ptw} + L_{tw} \qquad (3)$$

where

$$L_{tw} = K_1(\bar{T})\left[T_{tw} - T_a\right] + K_2(\bar{T})\left[T_{tw} - T_a\right] + K_3(\bar{T})\left[T_{tb} - T_{bb}\right] \qquad (4)$$

The summation term in equation (1) and (3) is replaced by a mean transmissivity, τ_s, in their actual evaluation. In nocturnal ascents these equations simplify because the lateral conduction terms are one order of magnitude smaller than the vertical conduction terms.

Equations (1) and (3) may be solved for the downward infrared flux, R_{id}.

$$R_{id} = \frac{1-r_i}{\tau_i(C_{sb}C_{iw} - C_{ib}C_{sw})}\left[C_{sb}C_{iw}B_{tw} - C_{ib}C_{sw}B_{tb} - \frac{\epsilon_i}{1-r_i}\left(C_{sb}C_{iw}B_{ptw} - C_{ib}C_{sw}B_{ptw}\right) + \frac{C_{sb}L_{tw} - C_{sw}L_{tb}}{1-r_i}\right] \qquad (5)$$

Equations (1) and (3) may also be solved for the downward short-wave flux, R_{sd}.

$$R_{sd} = \frac{C_{ib}C_{iw}(1-r_i)}{\tau_s C_{sb}C_{iw} - C_{ib}C_{sw}}\left[(B_{tb} - B_{tw}) - \frac{\epsilon_i}{1-r_i}\left(B_{ptb} - B_{ptw}\right) + \frac{L_{tb}}{C_{ib}(1-r_i)} + \frac{L_{tw}}{C_{iw}(1-r_i)}\right] \qquad (6)$$

Symmetric equations exist for the bottom radiometer surfaces so the upward radiation streams may be obtained in an analagous manner. The first and second terms on the left side of the equal

sign in equations (1) and (3) depict the short-wave and infrared radiation, respectively, absorbed by the sensing surface. The first term to the right of the equal sign in the same two equations represents the energy loss from the sensor surface by thermal radiation. The second term to the right of the equal sign introduces thermal radiation originating from the polyethylene. This term is usually very small; therefore, it is ignored in the actual radiation computations. The last terms in equations (1) and (3) are the conduction losses from the sensor surface due to top to air conduction.

2.5 Error Analysis

An error analysis on the system of equations used to solve for the downward short and infrared flux and upward infrared flux yields a standard error of $\pm$ .041 langley/minute in the infrared components and $\pm$ .068 in the downward short-wave component under cloudless conditions. The upward short-wave component is meaningless as the cosine response or the instrument is affected by the polyethylene's short-wave transmission. The standard deviation for nocturnal infrared measurements made by the radiometersonde is .007 langley/minute.

III. DESCRIPTION OF INSTRUMENT

Two economical radiometers, one with black sensor surfaces and the other with white surfaces, were flown on the same balloon package. Figure 4 is a schematic diagram of the net radiometer. The black surface coating was 9300-S Mautz black paint which exhibits a relatively high and constant spectral absorptivity. Two white surface coatings were tried, one using magnesium oxide and the other lead carbonate. Although magnesium oxide has more desirable spectral characteristics, the relative ruggedness and ease of application of lead carbonate make it a more desirable surface. The magnesium oxide was smoked on by burning magnesium ribbon at the lower end of a flue and placing the sensor at the top of the flue. The lead carbonate was applied in accordance with Brasefield's (1948) specifications. Due to transmission bands in the infrared spectrum of the white surfaces, a black undercoat was necessary. Figure 5 shows the infrared spectral absorptivities of 9300-S black paint (Kuhn, 1962), magnesium oxide with a 9300-S undercoat, and lead carbonate with a 9300-S undercoat.

The polyethylene shields on the top surfaces were supported by fine threads to maintain spacing necessary for the elimination of convection.

Another deviation from the normal construction of the radiometer was the mounting of the thermistors under the sensor surface to insure a flat surface. Otherwise, the bead thermistor on top

of the sensing surface presents a normal surface to the short-wave beam radiation. In dealing with isotropic radiation such as terrestrial radiation, the presence of the thermistor on top of the surface is unimportant. However, with the beam component of short-wave radiation, the exposure of a surface normal to the beam can disturb the geometry of the instrument.

IV. OBSERVATIONS AND RESULTS

Three daytime balloon radiometersonde flights have been made using the black-white radiometer system previously discussed. Two of these flights were made in Madison, Wisconsin, on August 22, 1963, and August 26, 1963. The other flight was made in Miami, Flordia, on April 1, 1964.

The white surface was lead carbonate in the Madison flights and magnesium oxide in the Miami ascent. One nighttime ascent was made with a conventional radiometersonde for comparison with the April 1, 1964, daytime sounding.

Since there is no reason to expect the downward infrared flux to change appreciably from day to night, assuming no air mass of cloud cover change, a comparison of the daytime and nighttime profiles is an indication of the reliability of the instrument. In the upward infrared flux profile one would expect higher values in the daytime because of a warmer surface temperature.

Figures 6 and 7 show the observed infrared profiles on April 1, 1964, at 0000 EST and 1200 EST, respectively. Throughout both flights the sky condition was reported as cloudless. During this twelve-hour period there was some moisture variation below 500 millibars. There was considerably more moisture during the nighttime ascent. Although the radiation profiles for the two flights are not identical, they do show distinct similarities. Calculated infrared profiles from the measured daytime moisture

distribution agree with the observed daytime infrared profile to within one standard error of the instrument. The similarity of the daytime and nighttime ascents clearly implies that a daytime infrared measurement under cloudless conditions is feasible.

Figures 8 and 9 illustrate the short-wave contamination of the infrared profiles by multiple reflection of the short-wave energy. As the radiometersonde approaches a cloud from below, the contamination first appears in the downward infrared flux measurement. Then as the radiometersonde enters the cloud layer, the upward infrared flux measurement is affected. In both of these flights the sky condition was reported by ground observers as 10/10 cirrus.

V. CONCLUSIONS

Three daytime balloon radiometersonde flights have been made using the black-white radiometer system previously discussed. Two of these flights were made in Madison, Wisconsin, on August 22, 1963, and August 26, 1963. The other flight was made in Miami, Florida, on April 1, 1964.

With a solar elevation angle greater than 50 degrees under cloudless conditions, the black-white radiometersonde can measure the infrared component of radiation to within a standard error of .061 langley/minute. Under the same conditions the downward short-wave component can be measured to within a standard error of .101 langley/minute. The upward short-wave radiation measurement is invalid because the angular dependence of the polyethylene transmission interferes with the cosine response of the instrument.

Under cloudy conditions and for solar elevation angles less than 50 degrees, the accuracy of the downward short-wave measurement is seriously affected. Probably by extending the white and black surface coatings to the rims of the respective radiometers, the infrared measurement would not be affected by the directional distribution of the short-wave energy. This concept will require testing.

REFERENCES

Beers, Y., 1957: Theory of Error. Reading, Massachusetts, Addison-Wesley Publishing Company, Inc., 66 pp.

Brasefield, C. J., 1948: Measurement of Air Temperature in the Presence of Solar Radiation. Journal of Meteorology, 5, pp. 147-148.

Carslaw, H. S., and J. C. Jaeger, 1959: Conduction of Heat in Solids. London, England, Oxford University Press.

Constant, F. W., 1959: Theoretical Physics. Reading, Massachusetts, Addison-Wesley Publishing Company, Inc., pp. 261-271.

De Graaf, J. C. A., and E. F. M. Van der Held, 1953: The Relation Between the Heat Transfer and the Convection Phenomena in Enclosed Plane Air Layers. Applied Sci. Research, 3A, pp. 393-409.

Kuhn, P. M., 1964: Personal communication with the author.

Schoffer, P., P. Kuhn, and C. M. Sapsford, 1961: Instrumentation for Solar Radiation Measurements. United Nations Conference on New Sources of Energy.

Suomi, V. E., D. O. Staley and P. M. Kuhn, 1958: A Direct Measurement of Infrared Radiation Divergence to 160 mb. Quarterly Journal of the Royal Meteorological Soceity, 84, pp. 134-141.

Tanner, C. B., J. A. Businger, and P. M. Kuhn, 1960: Economical Net Radiometer. Journal of Geophysical Research, 65, pp. 3657-3667.

Tanner, C. B., and P. M. Kuhn, 1962: Personal communication with the author.

Figure Legends

Figure 1. Lateral conduction in a typical nocturnal ascent.

Figure 2. Lateral conduction in a typical daytime ascent.

Figure 3. Polyethylene reflectivity as a function of solar elevation angle.

Figure 4. Schematic diagram of net radiometer.

Figure 5. Infrared absorptivities of sensor coatings (top to bottom): 9300-S Mautz paint; magnesium oxide with 9300-S undercoat; lead carbonate with 9300-S undercoat.

Figure 6. Infrared profiles observed in nocturnal ascent on 1 April 1964.

Figure 7. Infrared profiles observed in daytime ascent on 1 April 1964.

Figure 8. Infrared profiles observed in daytime ascent on 22 August 1964.

Figure 9. Infrared profiles observed in daytime ascent on 26 August 1964.

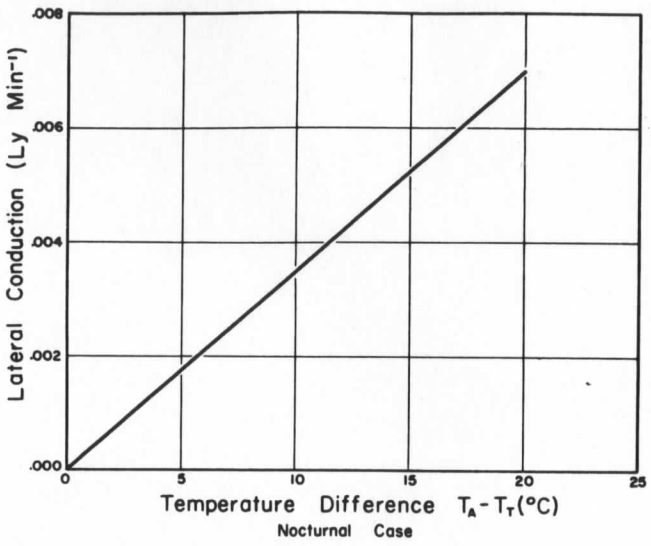
Lateral Conduction (Ly Min⁻¹)
.008
.006
.004
.002
.000
0
5
10
15
20
25
Temperature Difference $T_A - T_T$(°C)
Nocturnal Case

Fig. 1.

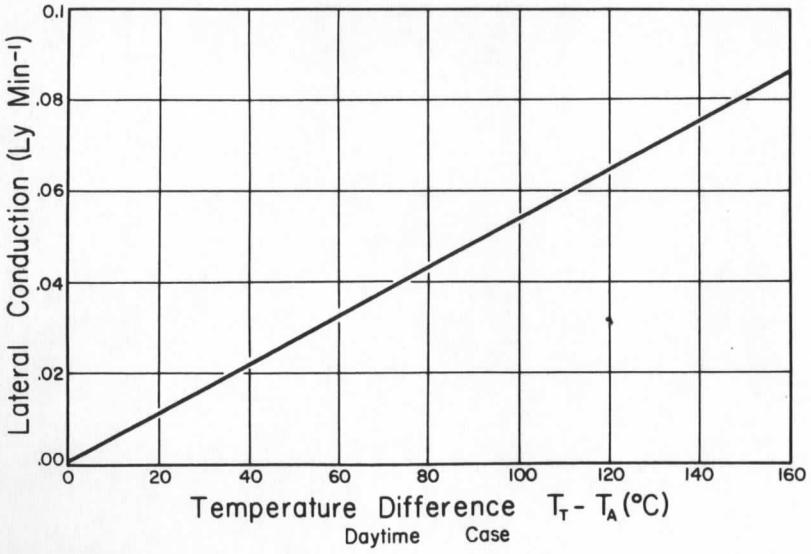
Lateral Conduction (Ly Min⁻¹)
0.1
.08
.06
.04
.02
.00
0
20
40
60
80
100
120
140
160
Temperature Difference $T_T - T_A$(°C)
Daytime Case

Fig. 2.

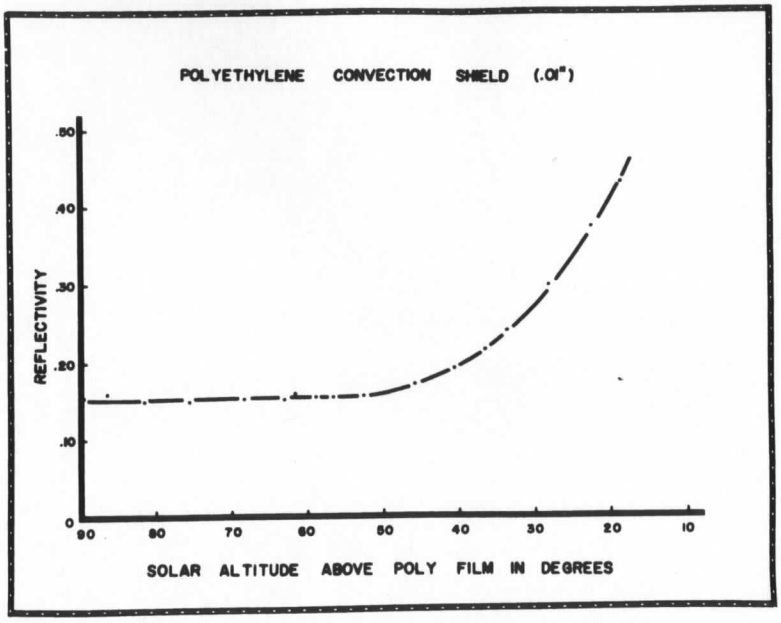
POLYETHYLENE CONVECTION SHIELD (.01")
REFLECTIVITY
.50
.40
.30
.20
.10
0
90
80
70
60
50
40
30
20
10
SOLAR ALTITUDE ABOVE POLY FILM IN DEGREES

Fig. 3.

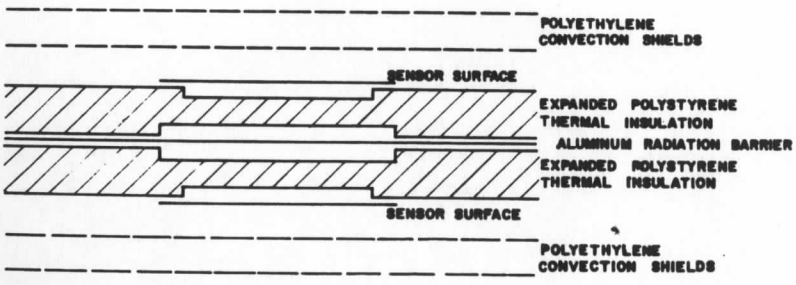
POLYETHYLENE
CONVECTION SHIELDS
SENSOR SURFACE
EXPANDED POLYSTYRENE
THERMAL INSULATION
ALUMINUM RADIATION BARRIER
EXPANDED POLYSTYRENE
THERMAL INSULATION
SENSOR SURFACE
POLYETHYLENE
CONVECTION SHIELDS

Fig. 4.

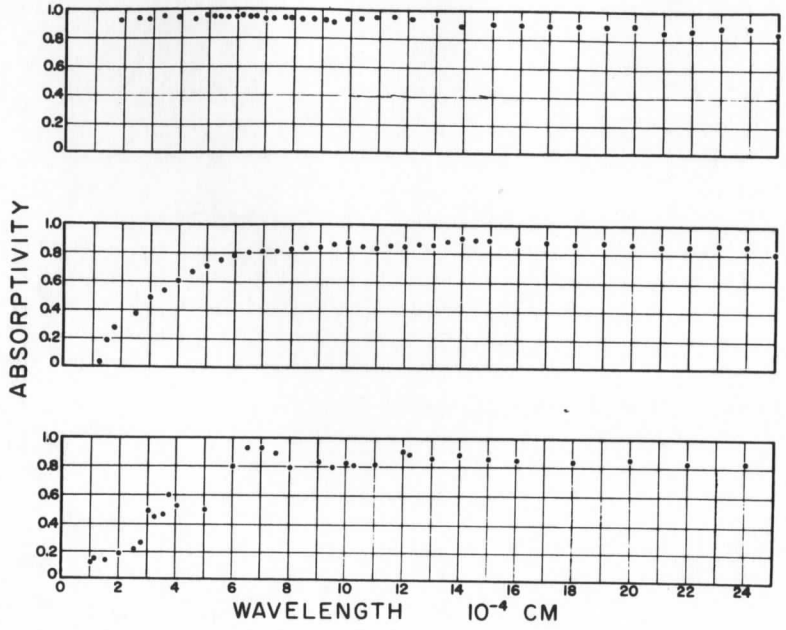
ABSORPTIVITY
1.0
0.8
0.6
0.4
0.2
0
0 2 4 6 8 10 12 14 16 18 20 22 24
WAVELENGTH 10^{-4} CM

Fig. 5.

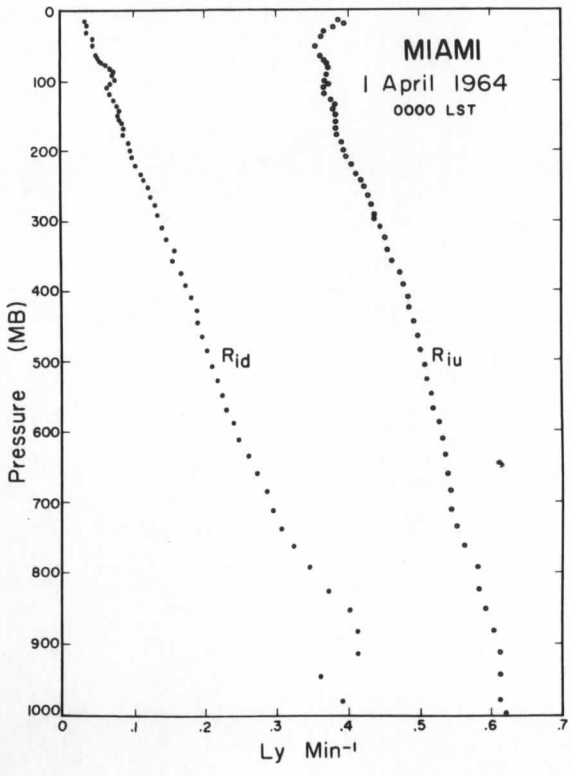
MIAMI
1 April 1964
0000 LST
R_{id}
R_{iu}
Pressure (MB)
0 100 200 300 400 500 600 700 800 900 1000
0 .1 .2 .3 .4 .5 .6 .7
Ly Min^{-1}

Fig. 6.

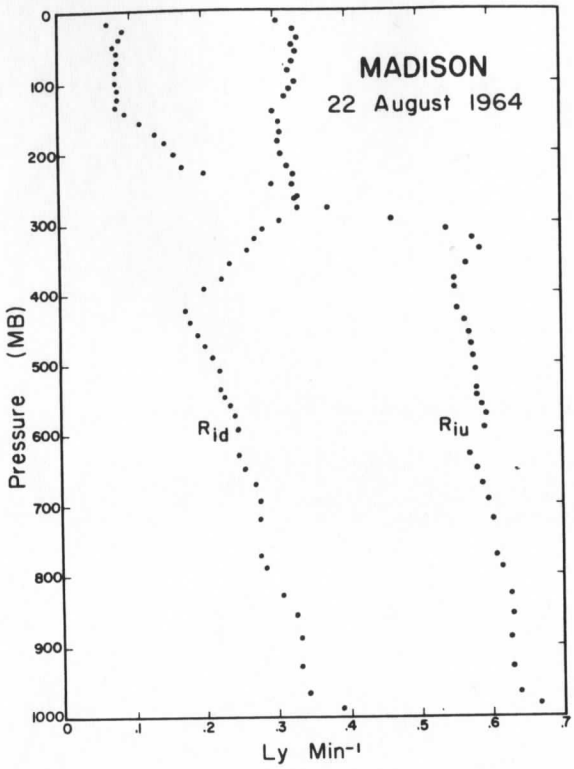
MADISON
22 August 1964
Pressure (MB)
0
100
200
300
400
500
600
700
800
900
1000
R_{id}
R_{iu}
0
.1
.2
.3
.4
.5
.6
.7
Ly Min^{-1}

Fig. 8.

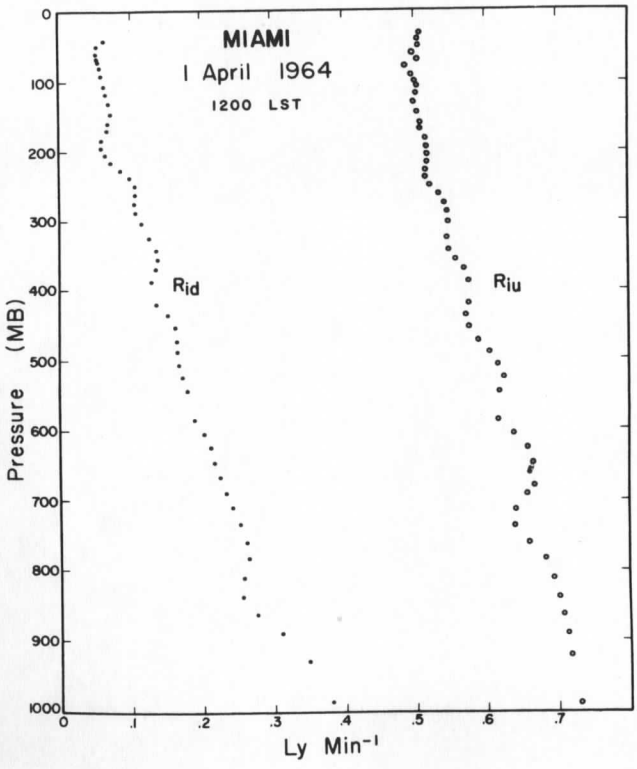
MIAMI
1 April 1964
1200 LST
Pressure (MB)
0
100
200
300
400
500
600
700
800
900
1000
R_{id}
R_{iu}
0
.1
.2
.3
.4
.5
.6
.7
Ly Min^{-1}

Fig. 7.

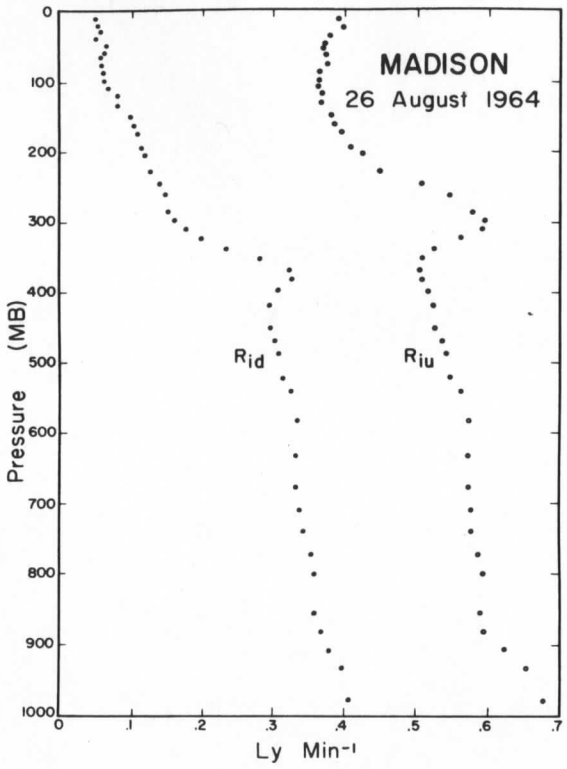
MADISON
26 August 1964
Rid
Riu
Pressure (MB)
0
100
200
300
400
500
600
700
800
900
1000
0
.1
.2
.3
.4
.5
.6
.7
Ly Min-1

Fig. 9.

6. RADIOMETERSONDE SCIENTIFIC MANUAL

P.M. Kuhn and V.E. Suomi

A scientific manual for the radiometersonde is currently being produced. This manual will be published shortly under separate cover as a scientific manual of the USWB. It will contain the following topics:

1. Introduction
2. Physical Description of the Radiometer
3. Radiometer as Part of a Sounding System -- The Radiometer Sonde.
4. Processing of Radiation Output Data (Co-author D. Johnson)
5. Computer Programs for Data Reduction
6. Accuracy of Measurements
7. Limitations of Radiometer (Author S.K. Cox)
8. Typical Radiation Soundings
9. Appendix

7. SUMMARY OF CURRENT RESEARCH

The compilation of notes relating those research topics which were initiated or continued during the reporting period but which have not yet resulted in publications or have not reached a final stage is contained in this chapter. Since many of these topics are pursued by more than one researcher, no names of specific investigators have been attached to the various topics. Results of these investigations will be made available whenever feasible.

a. Infrared Flux Soundings and Calculations through an Atmosphere with Clouds.

Recent infrared flux soundings in an atmosphere with clouds show considerable variation in the measured "blackness" of high and middle clouds. A radiative transfer model incorporating variable cloud "blackness" or effective emissivity and variable cloud height is shown to yield fluxes in better agreement with simultaneous flux soundings (obtained from radiometersonde and other radiometers) than previous models. The earlier models assumed totally opaque or 50 per cent opaque cloud layers.

In the model being tested, flux emissivities, integrated over all wave numbers, determine the upward and downward flux. The obvious advantage of the use of flux emissivities rather than spectral band transmissivities, in radiation study is, as Dr. George J. Haltner and Dr. F. L. Martin have stated (1957), that direct radiometric measurements, in situ, of the flux or intensity can and have been made. Such measurements (Kuhn, 1962) are being used in this study as the basis of a transfer model.

The equation for the upward flux developed for this model is

$$F\uparrow = \sum_{i=1}^{M} F_{B_{i-1/2}} \Delta\epsilon_{i_w} + \sum_{j=1}^{N} F_{B_{j-1/2}} \Delta\epsilon_{j_c} + \left(1.0 - \sum_{i=1}^{M} \Delta\epsilon_{i_w} - \sum_{j=1}^{N} \Delta\epsilon_{j_c} + \sum_{i=1}^{M}\sum_{j=1}^{N} \Delta\epsilon_{i_w} \Delta\epsilon_{i_c}\right) \times \left(\epsilon^* F_2\uparrow + (1-\epsilon^*) F_1\uparrow\right)$$

where F is flux, ϵ is flux emissivity, ϵ^* is effective cloud flux emissivity. The subscript B means black body, i and j are

indexing variables, w means water vapor, and c is carbon dioxide. Solutions of the equation are obtained numerically on IBM 1410 and CDC-3600 computers of the Wisconsin Computing Center.

Research in progress shows that radiative flux computed by means of Equation (1), under the assumption of no clouds, is essentially identical to flux computed by means of a transfer model summing partial fluxes using laboratory determined band transmissivities. The latter method employs the following form of the transfer equation,

$$F\uparrow = -\sum_{0}^{\infty} F_{B}\uparrow \Delta\lambda + \sum_{0}^{\infty}\sum_{i=1}^{n} \tau_{i-1/2}\, \Delta F_{B_i}\, \Delta\lambda$$

where t is the transmissivity, T the temperature and i and v are indexing variables. Equation (2) was, of course, solved (as is Equation (1)) for each of the optically active atmospheric gases and for window transmissivity.

Cloud emissivity classes were chosen for stratus, alto stratus or cumulus, and cirrostratus or cirrus. Sky cover was divided into three classes, namely, scattered (20%), broken (50%), and overcast (100%). Presently a "climatology" of cloud emissivities, related to surface or TIROS satellite observations, and, in many instances, verified by observers in high flying jet aircraft is being developed.

Preliminary calculations of upward and downward flux by equation (1) in cloudy atmospheres with observer verification of the clouds show that concurrent flux observations agree with the

calculations. This will include instances of jet aircraft observation verification of very high thin clouds. The U-2 aircraft study described in the next subsection (b), is closely related to this work as is the Infrared Radiation Model Atmosphere w th Infrared Observations for Input Data study, described in subsection (c).

b. Measurement of the Composition of Infrared Attenuating High Pariculate Strata

This study, the feasibility of which was discussed in Section 4 above, has now reached the first environmental test stages for the two Barnes Radiometers. The radiometers will be mounted in the AFCRL instrument panel of the U-2 aircraft and preliminary flight testing is planned for late 1964.

The second of the two radiometers will carry the saphire cutoff filter (1λ- 5.5λ) discussed in Section 4, while the first or original radiometer will have the 7λ - 13λ band pass filter with its optics. The radiometers will be calibrated for an environmental temperature of -40.0°C and a target (surface) temperature of approximately +35.0°C.

c. Transfer Model of the Atmospheric Heat Balance

The close relationship between the study of subsection (a) and this research is evident. Although a paper on subsection (a) is in process, it is presently planned to combine this Heat Balance work with the transfer model study involving a cloudy atmosphere.

A unique feature of this study is that, while a transfer model is developed, the controlled input has been obtained from actual observations of the radiative flux. The flux emissivities required in the solution were actually taken "in situ" during our atmospheric radiometric soundings.

d. "Piggyback" Radiometersonde Ascent (U.S. Weather Bureau Satellite Infrared Spectrometer)

Radiometersonde data from the September, U. S. Weather Bureau SIRS high level balloon ascent at Palestine (NCAR) Texas to San Angelo, Texas is being reduced. The balloon flight continued from forty minutes before sunrise for 7½ hours. For the first time directly downward facing cameras operated throughout a radiometersonde flight. The radiometersonde data was recorded for the full 7½ hours and correlations between up-swelling cumulus and upwelling radiation changes are now being developed.

The upward facing radiometer* employed the new 62 mil polyethylene diffusing window. A careful test of this potentially valuable surface is being made. The special white upward facing sensing surface is to be carefully checked for future use.

The downward facing radiometer has essentially the same configuration as in current two year old models, except that a better thermistor circuit for linearity was employed. Data are being reduced to radiant fluxes.

*This radiometer, developed by Suomi-Kuhn, will be called the "Wisconsin radiometer" in subsequent paragraphs.

e. Munich Intercomparisons

All data from the Munich, December 1963 ascents have been reduced and comparison studies are being concluded. A report and paper will be issued. Of principal importance are the following conclusions now being finalized:

(1) The Müller-Pohl (Munich) sonde in its 1963 configuration was not satisfactory in a cloud and generally snow-filled troposphere.

(2) The Munich and Wisconsin sondes agreed in general in the stratosphere.

(3) The Wisconsin radiometers tracked on the downward flux above 150 millibars from ascent to ascent at night separated by approximately three hours. This study is encouraging as it develops.

(4) A further comparison between Russian, Japanese, German (Munich) and the Wisconsin radiometers is being planned for Madison and Miami in 1965. IAMAP president F. Möller has asked P. M. Kuhn to serve as convenor. Dr. Kuhn will coordinate this international mission with the appropriate authorities.

f. In-Flight Photography of the Radiometersonde

In a continuing study of possible condensation effects on the upper polyethylene ventilation shields of the Wisconsin radiometersonde, the first in-flight observations indicate no surface condensation during a seventy-minute ascent in a cloudless sky. The ascent was made by NCAR at Palestine, Texas.

A second ascent into winter time stratus and alto stratus clouds is being prepared. Photographic results during the first flight were excellent and essentially the same procedure will be followed for the succeeding ascents.

g. Cold Chamber Study of Radiative Effects of Aerosols on Incident Radiation

At present a cold chamber for the generation of ice crystals with a Tessla coil silver iodide generator has been completed. A source for infrared radiation and a suitable radiometric sensor to measure scattered radiation from the ice aerosol to be used inside the cold chamber is under study.

h. Cloud Height from Radiosonde Adjusted Satellite Infrared Observations

Troposphere to low stratosphere vertical atmospheric temperature and cloud structure reproduction from TIROS satellite infrared observations has posed certain problems, especially during nighttime observations. A computer procedure for utilizing radiosonde observations within a limited time of and a limited distance from a satellite infrared observation to assist in calculating actual cloud height has been developed. Radiative transfer theory links the satellite observation to the radiosonde vertical probe to provide a more refined vertical temperature and cloud profile than can presently be obtained from TIROS infrared observations alone in the atmospheric window and broad channels.

A preliminary report on first results of this technique was presented at the AMS meeting at Atlantic City in March, 1964. The anomalies between observed satellite upwelling flux and computed upward flux after insertion of a cloud are largely reduced except for satellite sensor degradation. Continuing work towards a final paper is in progress.

i. Optical Cloud Detectors

Devices to obtain synoptic measurements on the density of light scattering aerosols and clouds from routine sonde ascents are under development. Criteria incorporated in the design of such devices are light weight, low cost and expendability. Devices suitable for the measurement of sunlight reflected 15° above the horizon have been flown. These devices were carried aboard airplanes; entrance into and emergence from cumulus clouds was readily observed with these devices. Balloon flights demonstrated that these devices indicated the presence of clouds. The existance of these clouds could be correlated with humidity measurements from ground to altitudes near the 400 mb level. Another type of balloon borne sensor measuring the sunlight reflected from 35° above the horizon is being tested to measure the optical density and altitude of aerosols and tenuous cirrus clouds. Low-cost, balloon-borne aerosol sensors for nocturnal ascents are also under development. Present units have detecte dust and pollen present near the ground on clear nights.

These units should yield information to supplement radiometersonde measurements. These units should also aid high flying aircraft by measuring horizontal visibility at altitudes up to 30 km.

j. Density Gauge

A thermionic air density gauge is under development. Such gauges have response times less than 10^{-4} sec. The present unit has a pre-specified nearly linear response for densities corresponding to $10^{-3} \leq P \leq 10$ mb at 20° C. The shape of the calibration curve can be varied by choice of associated circuit components. Most problems associated with the operation of a thermionic electron device in an oxidizing atmosphere at relatively high pressures (P near 10 mb) have been overcome. However thermal expansion of grid wires changes the dimensions of the gauge thereby rendering the density measurements somewhat unreproducible. The gauge is currently being redesigned to overcome this defect.

8. Appendix

MEASURED EFFECTIVE LONG-WAVE EMISSIVITY OF CLOUDS

P. M. KUHN
U.S. Weather Bureau, The University of Wisconsin, Madison, Wis.
[Manuscript received July 2, 1963; revised September 9, 1963]

ABSTRACT

Measurements of the effective long-wave emissivity of clouds, equivalent to one minus the slab transmissivity, are obtained through thermal energy relations at cloud tops and bases after the manner of Gergen. Radiometric measurements are employed. Aircraft-verified cloud heights and measured effective cloud emissivities provide a basis for determining the presence of middle and high clouds. Such clouds result in large changes in radiation flux and apparent earth temperature measurements from satellites and high level balloons.

Symbol	Definition	Appears in equation
$F_1\downarrow$	Downward long-wave radiative flux, level 1	1
$F_1\uparrow$	Upward long-wave radiative flux, level 1	1
$F_2\downarrow$	Downward long-wave radiative flux, level 2	2
$F_2\uparrow$	Upward long-wave radiative flux, level 2	2
F_{E1}	Equivalent long-wave radiative flux, level 1	1, 6
F_{E2}	Equivalent long-wave radiative flux, level 2	2, 6
ϵ^*	Effective long-wave cloud emissivity	3, 6
F_{c1}	Long-wave radiative flux from cloud, level 1	1
F_{c2}	Long-wave radiative flux from cloud, level 2	2
F_{B1}	Equivalent long-wave radiative flux, cloud assumed black, level 1	4, 6
F_{B2}	Equivalent long-wave radiative flux, cloud assumed black, level 2	5, 6
$F\uparrow$	Upward long-wave radiative flux	7
u	Optical depth (cm.) of absorbing gas	7
σ	Stefan-Boltzman constant, 0.817×10^{-10} cal./cm.^{2} min. deg.^{4}	7
$\bar{T}$	Mean air temperature (°K.) of atmospheric layer	7
$(u)_w$	Optical depth of atmospheric water vapor (precipitable centimeters)	7
$(u)_c$	Optical depth of atmospheric carbon dioxide (atmospheric centimeters)	7
$(u)_o$	Optical depth of atmospheric ozone (atmospheric centimeters)	7
T_0	Earth's surface temperature (°K.)	7

1. INTRODUCTION

Measurements of the long-wave emissivity or transmissivity of clouds above the earth's surface are difficult and, consequently, scarce. Notable among measurements of long-wave transmissivity of clouds are those of Gergen [4], Gates and Shaw [3], and Brewer and Houghton [1]. However, the importance of the transmission properties of clouds to infrared satellite and balloon measurements of the atmosphere, is well known. The thermal energy exchange between the earth, the atmosphere, and space is strongly influenced by cloud cover. Opaque (to long-wave radiation) cloud layers provide a high cold radiating source near their tops for upward-streaming radiation above the clouds. On the other hand, thermal energy considerations must include the transmissivity or emissivity of clouds that are not opaque. For here radiation above the clouds comes not only from the clouds but also from earth and atmosphere beneath. Gates and Shaw [3] outline the problems in obtaining measurements of cloud emissivity requiring observations of drop size distribution and concentration in the cloud, cloud thickness, and cloud composition. The inaccessibility of the clouds and the compound instrument problem have required aircraft or large balloon probes.

Following the general principles of a procedure developed by Gergen [4] in his "black ball" experiments for the determination of "blackness" of clouds, but using observed upward and downward flux rather than calculated, it was possible to make several measurements of the long-wave emissivity of clouds. The radiometersonde (Suomi and Kuhn [11]) is well suited for such measurements, since it has been aloft through most cloud types. Aircraft verifications of the actual bases and tops of the clouds under observation were obtained, and all measurements were at night.

The principal purpose of the research described is to measure the effective long-wave emissivity of clouds. This may be subdivided into the location of cloud layers by infrared observations; the measurement of their effective emissivity, one minus the cloud's slab transmissivity; and the application of high and middle cloud emissivity in analyzing satellite infrared observations.

The method of accomplishing the purposes of the research is best summarized in the research technique.

First, the effective long-wave emissivity includes both the actual cloud emissivity and the cloud scatter effects and is defined by ϵ^*, equivalent to one minus the slab transmissivity. To obtain the effective infrared emissivity of clouds we measure the equivalent infrared flux, defined as one-half the sum of the upstreaming and downstreaming radiant flux at a plane in the atmosphere parallel to the earth's surface, in this case a cloud top or base. By considering the thermal energy budget at the base and top of a cloud the observed fluxes algebraically reduce to the above-defined cloud emissivity.

Having observations of cloud emissivities one may cal-

704-966—63——11

culate the upward flux of infrared radiation at satellite vel in the presence of clouds by means of one of the various forms of the transfer equation. A review of observations of TIROS infrared data has illustrated effects of clouds and possible atmospheric particulates. The 7–30-micron broad response channel on TIROS, as well as the 8–12-micron "window" channel have shown large changes in the apparent earth temperature. McGee [8] and Wark, Yamamoto, and Lienesch [12] have noted that in many cases these appear to be related to the presence of clouds. Such clouds can be high cirrus, unseen from the ground. Riehl [9] speaks of strong radiative cooling in the Caribbean, and Gergen [5] notes that an observation of high clouds with a transmissivity of 71 percent produces a 35 percent attenuation of the upward-streaming flux. Radiometersonde measurements have shown similar attenuations. With satellite observations of the upward flux and an atmospheric (radiosonde) sounding from the same area, it is possible to employ measured effective emissivities in adjusting the calculated flux to equal the observed. This is accomplished by interposing a "black" or "gray" cloud at selected heights, the cloud's effect being that of attenuation and re-radiation at lower temperatures. Thus, while qualitatively it is well known that "unseen" high clouds may greatly reduce the magnitude of the upward flux, this procedure apparently provides a quantitative measure of the effects of oud emissivities on certain satellite measurements.

2. INSTRUMENTAL PROCEDURE

For these emissivity measurements, it was necessary to secure measurements of the height of both the cloud bases and tops as well as a complete vertical radiation profile in the infrared through the cloud. The radiometersonde (Kuhn [6], Bushnell and Suomi [2]) was the infrared radiation probe. Aircraft observations of cloud bases and tops for each of four cloud situations gave the necessary data on the vertical distribution of the clouds. It will be shown, as Gergen [4] did previously, that vertical profiles of the equivalent radiation (defined above) can indicate cloud bases and tops.

3. EMISSIVITY CALCULATIONS

From figure 1, indicating the distribution of radiative fluxes above and below a cloud layer in the atmosphere, we can form the equations for the thermal energy transfers at the top and base of the cloud. Let us suppose that a cloud layer between levels 1 and 2 has a gray body effective emissivity ϵ^*. At the level 1 there are two radiation currents contributing to the equivalent radiation, F_E, namely, $F_1\downarrow$ and $F_1\uparrow$. Similarly at level 2 we have $\downarrow$ and $F_2\uparrow$. We may form the equations

$$2F_{E1}=F_1\downarrow+F_1\uparrow=(1-\epsilon^*)F_2\downarrow+\epsilon^*F_{c1}+F_1\uparrow \quad (1)$$

$$2F_{E2}=F_2\downarrow+F_2\uparrow=(1-\epsilon^*)F_1\uparrow+\epsilon^*F_{c2}+F_2\downarrow \quad (2)$$

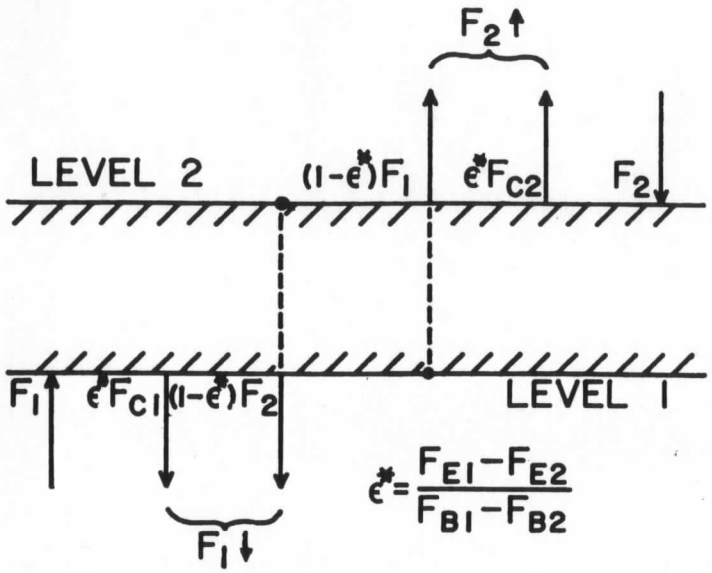

FIGURE 1.—Cloud layer and associated radiative fluxes.

where

$$F_1\downarrow=(1-\epsilon^*)F_2\downarrow+F_{c1} \quad \text{and} \quad F_2\uparrow=(1-\epsilon^*)F_1\uparrow+F_{c2}$$

Subtracting equation (2) from equation (1) we obtain:

$$2F_{E1}-2F_{E2}=-\epsilon^*F_2\downarrow+\epsilon^*F_1\uparrow+\epsilon^*F_{c1}-\epsilon^*F_{c2} \quad (3)$$

A simple consideration of the energy transfers at the cloud top and base, assuming the cloud to be black, while considering similar actual observations of a "gray" cloud, leads one to believe that a relatively simple algebraic relationship between equations similar to (1) and (2) would provide the effective cloud emissivity. In effect we compare energy transfers for a gray and a black cloud by means of the ratio of equivalent radiations for the gray and the assumed black cloud.

The equivalent radiation for a black cloud, symbolized by F_B instead of F_E, is defined as one-half of the sum of the black body radiation, F_c, at the base or top of a cloud and $F_1\uparrow$ or $F_2\downarrow$. Then we may write:

$$2F_{B1}=F_{c1}+F_1\uparrow \quad (4)$$

$$2F_{B2}=F_{c2}+F_2\downarrow \quad (5)$$

Substituting equation (4) and (5) in equation (3) we obtain:

$$\epsilon^*=(F_{E1}-F_{E2})/(F_{B1}-F_{B2}) \quad (6)$$

To review, $F_1\uparrow$, $F_1\downarrow$, $F_2\uparrow$, $F_2\downarrow$ are all measured quantities. Actually F_{c1} and F_{c2} are measured in that their temperatures are also measured. It should also be noted that the water vapor flux emissivity is accounted for in the equations and does not affect the measured effective cloud emissivity.

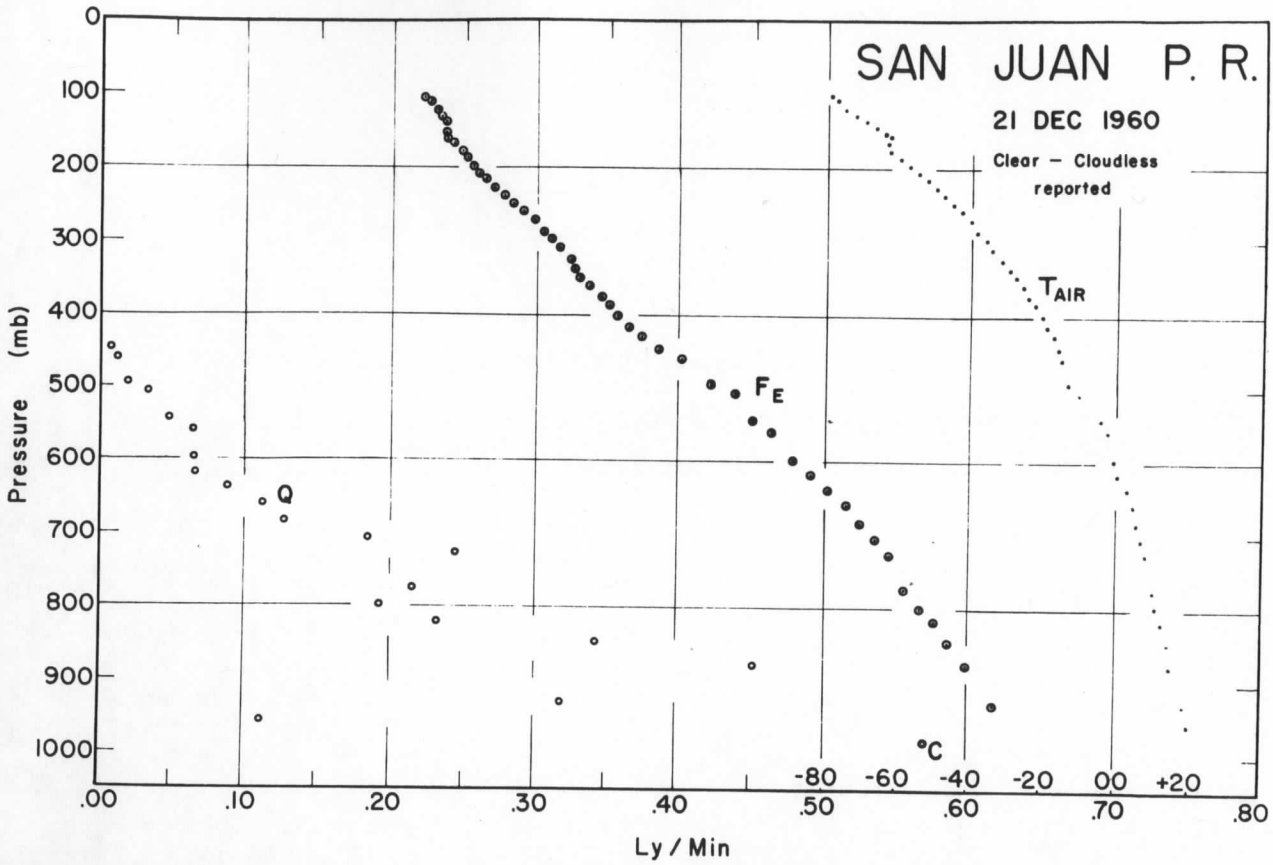

FIGURE 2.—Equivalent radiation, F'_E, air temperature T_{AIR}, and mixing ratio Q, San Juan, P.R., December 21, 1960.

4. RESULTS OF EMISSIVITY MEASUREMENTS

Figures 2 through 6 summarize the cloud emissivity observations. Certain conclusions can be drawn. Figure 2 demonstrates an essentially linear plot of the equivalent radiation for a reported cloudless sky at San Juan, P.R., on December 21, 1960. In each of figures 2 through 6 the ordinate is pressure on a linear scale and the abscissa has two scales, one for temperature in degrees Celsius and the other for radiation in langleys per minute.

In figure 3 for Madison, Wis., the observed cloud top and base are indicated. The equivalent radiation profile changes abruptly at 900 mb., the cloud base, and then resumes its previous lapse abruptly at 855 mb., the cloud top. The solution of equation (6) gives an emissivity of 0.98 for this 10/10 stratocumulus cloud. As a result of inaccuracies in the measurement of the exact height of the cloud bases and tops, it is possible for the effective emissivity, ϵ^*, to exceed 1.00 by a small amount. Two standard errors in radiometersonde-measured upward or downward flux are equivalent to 0.006 ly. min.$^{-1}$ (4.2 watts m.$^{-2}$). This random error effect may result in a ± 7 percent error in the effective cloud emissivity.

Figure 4 illustrates an observed 9/10 altocumulus cloud layer at Peoria, Ill., on Jan. 13, 1961. Observations of the equivalent radiation profile give an effective cloud emissivity of 60 percent by equation (6). In all figures the Q, or mixing ratio, curve is given in grams per kilogram and utilizes the numerical values of the radiation scale. It is interesting to see the mixing ratio decrease through the cloud, from 570 through 490 mb. in this example.

The two examples in figures 5 and 6 illustrate the emissivity determinations for observed middle and high clouds. Figure 5 illustrates altocumulus clouds overlain by cirrostratus sheets with tops at 250 mb. The multilayer effect reduces, somewhat, the sharpness of the change in the equivalent radiation profile. Emissivity evaluation by equation (6) gives 75 percent for this relatively deep cloud. In figure 6, the only verified example of a high cirrostratus sheet, 9/10 overcast, the profile of equivalent radiation is almost discontinuous at 235 mb. and at 160 mb., the cirrus top. Emissivity was calculated to be 59 percent.

From the four verified cloud observations we have obtained a range in the effective long-wave cloud emissivities of from 98 percent for low stratiform clouds to 59 percent for a 9/10 cirrostratus sheet. Among the 75 emissivity computations made without aircraft verification of cloud bases and tops, the emissivities for all cloud types range from 10 to 100 percent. The latter calculations, based upon ground cloud observations, and with bases and tops of clouds located by the equivalent radiation profile, provided cirrus emissivities for 55 cases.

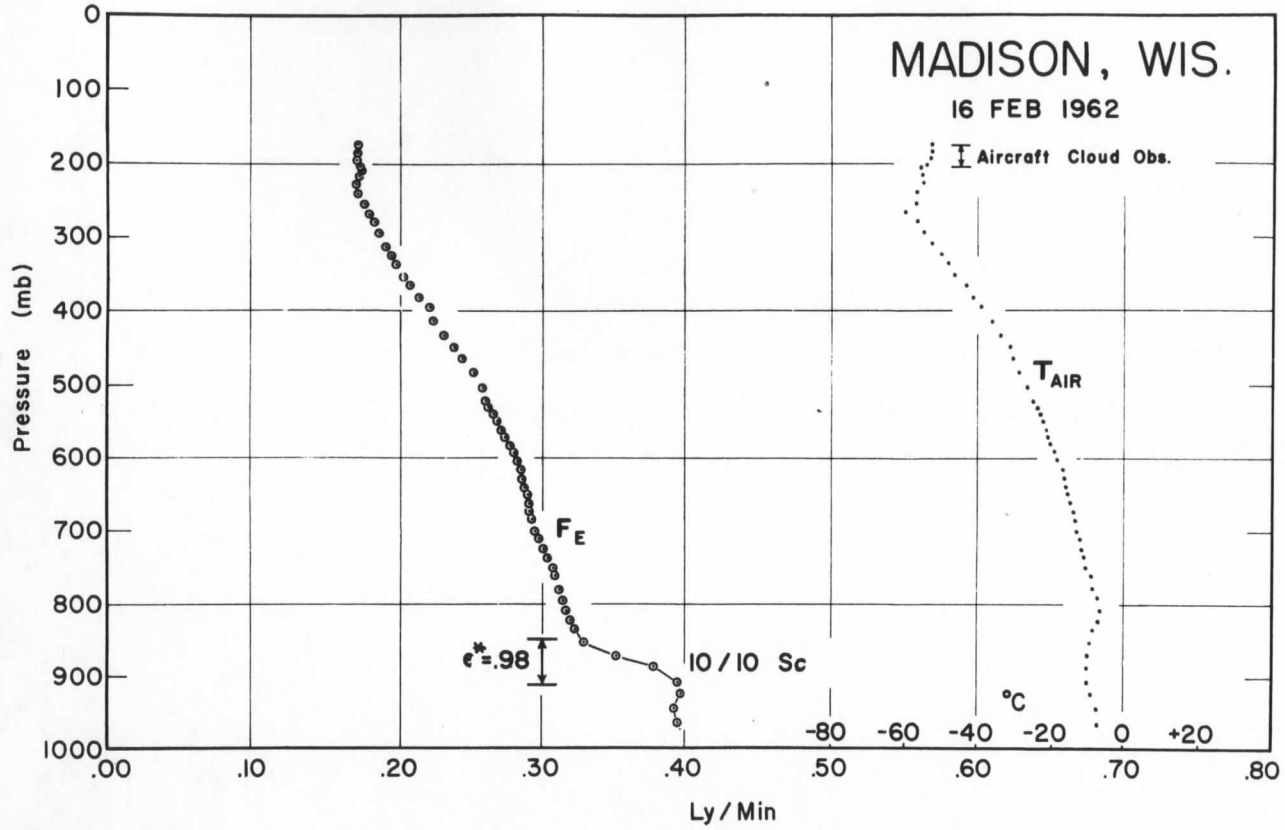

FIGURE 3.—Equivalent radiation, F_E, air temperature, T_{AIR}, and mixing ratio, Q, Madison, Wis., February 16, 1962.

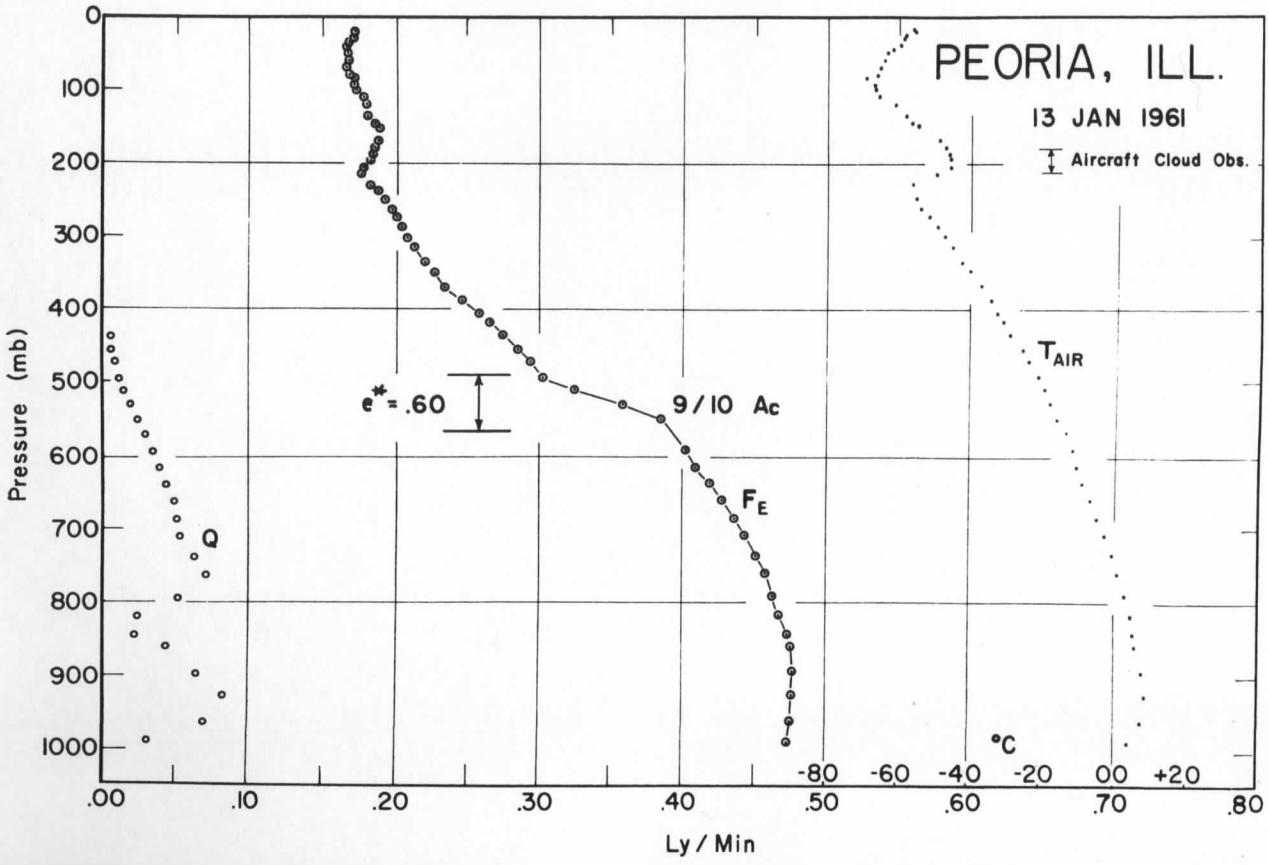

FIGURE 4.—Equivalent radiation, F_E, air temperature, T_{AIR}, and mixing ratio, Q, Peoria, Ill., January 13, 1961.

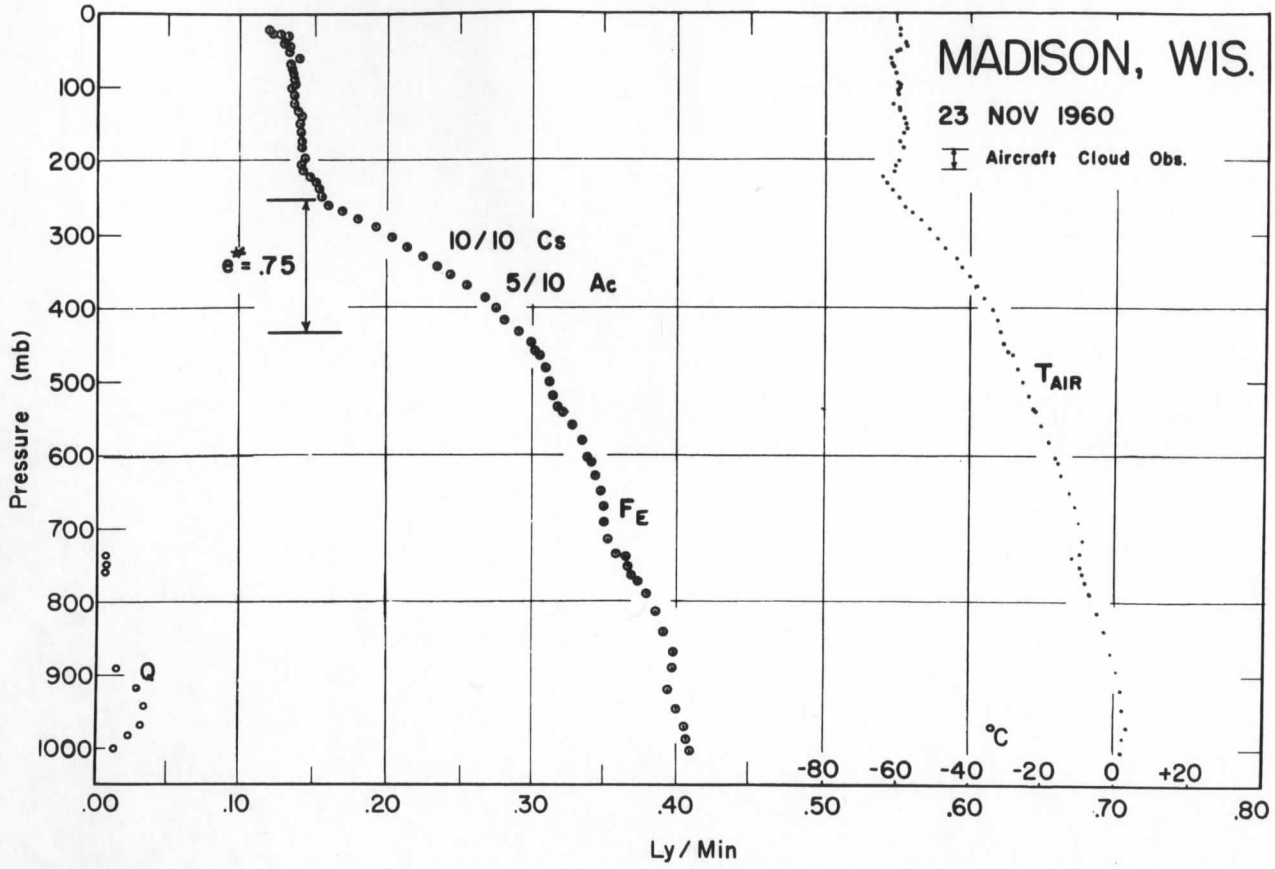

FIGURE 5.—Equivalent radiation, F_E, air temperature T_{AIR}, and mixing ratio, Q, Madison, Wis., November 23, 1960.

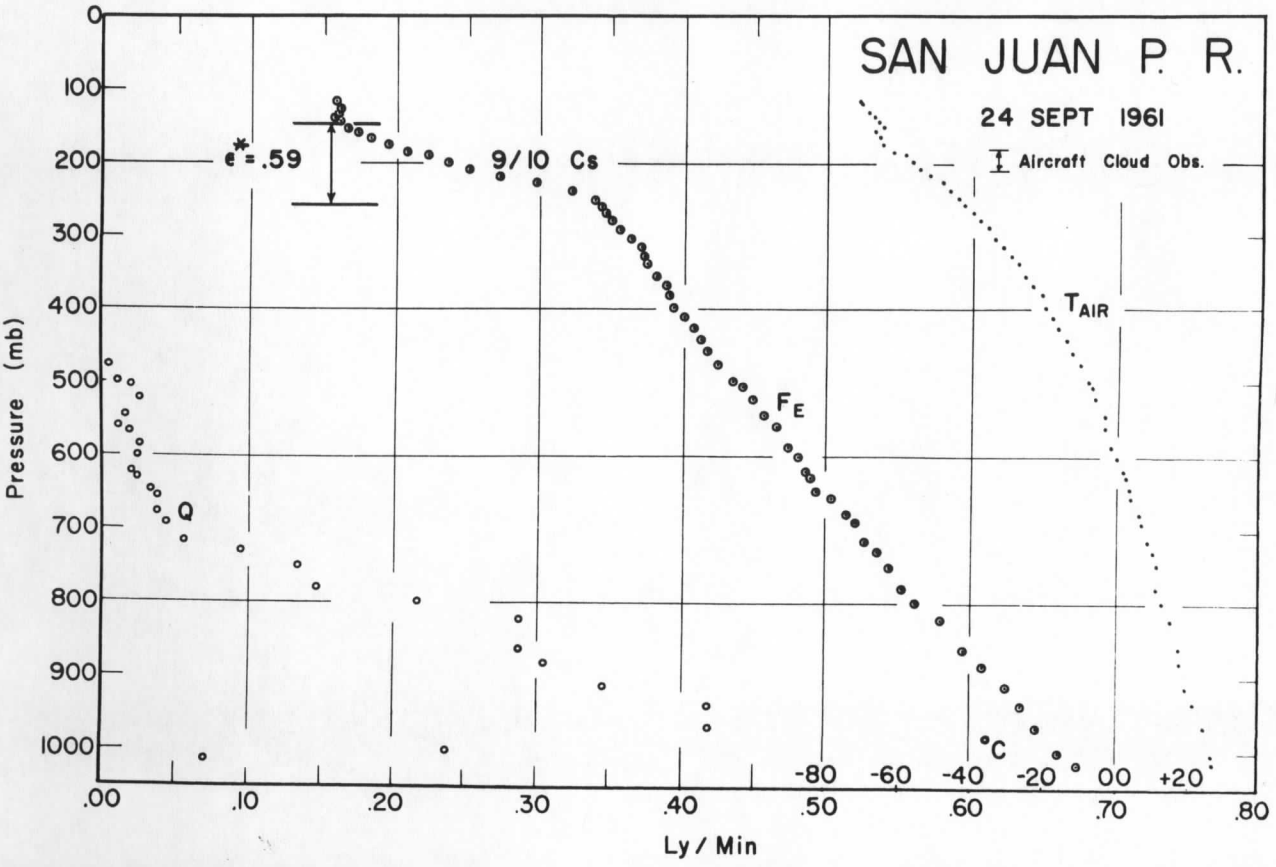

FIGURE 6.—Equivalent radiation, F_I, air temperature, T_{AIR}, and mixing ratio, Q, San Juan, P.R., September 24, 1961.

...n cirrus emissivity range was from 10 to 75 percent, in general agreement with findings of Brewer and Houghton [1] from airborne bolometer measurements at cloud bases and tops. Potentially this method affords an important tool for a climatology of cloud type emissivities.

5. CLOUD EFFECTS ON SATELLITE RESULTS

The transfer equation employing flux emissivities over isothermal atmospheric layers provides a calculation of the upward infrared flux from conventional radiosonde information for comparison with TIROS II outgoing radiation measurements. The transfer equation for upward flux at a reference level in the atmosphere is given by

$$F\uparrow = \int_0^u \sigma \overline{T}^4(u)_w (\partial \epsilon_f(u)_w/\partial u)du + \int_0^u \sigma \overline{T}^4(u)_c (\partial \epsilon_f(u)_c/\partial u)du + \int_0^u \sigma \overline{T}^4(u)_o (\partial \epsilon_f(u)_o/\partial u)du + \left(1.0 - \int_0^u (\partial \epsilon_f(u)_w/\partial u)du - \int_0^u (\partial \epsilon_f(u)_c/\partial u)du - \int_0^u (\partial \epsilon_f(u)_o/\partial u)du\right)\sigma T_0^4 \quad (7)$$

The use of equation (7) in computing radiative flux by numerical techniques is described in textbooks dealing with radiant energy transfer. A recent use is described by Kuhn [7]. Effects of overlap in the 15.0-micron carbon dioxide band and the rotational water vapor band were minimized by reducing the carbon dioxide flux emissivities by 12 percent.

Two examples of cloud effects on TIROS outgoing radiation flux observations over International Falls, Minn., are cited. The satellite measurements of upward flux and the synoptic cloud observations were furnished by Soules [10]. On December 23, 1960 at 2100 LST the satellite sensors over International Falls observed an outward flux of 0.243 ly. min.$^{-1}$ At this time the total sky cover was 10/10 with 4/10 opaque sky cover. The calculated outward flux from equation (7), not considering clouds, is 0.272 ly min.$^{-1}$ employing the International Falls 1800 LST radiosonde data for this date. Recalculating the upward flux by equation (7) after interposing a 60 percent "black" cirriform cloud at 6.7 km., at measured air temperature, gives a calculated flux of 0.235 ly. min.$^{-1}$, in close agreement with the measured flux. The determination of the 6.7 km. cloud height was accomplished by successive computer trial computations. Cloud attenuation of the upward-streaming radiation is evident from the fact that transfer equation calculations based upon the atmospheric water vapor and carbon dioxide, alone, gave significantly larger upward flux calculations than the flux observed from the TIROS satellite. Only after a gray cloud interposed did the two fluxes agree.

On January 16, 1961, at 1600 LST, during a pass over International Falls, the TIROS II infrared sensors measured an outward flux of 0.250 ly. min.$^{-1}$ Calculating the upward flux after interposing a 60 percent "black" cloud at 7.3 km. reduced the previously calculated flux without presence of cloud to 0.255 ly. min.$^{-1}$ Again cloud attenuation is evident. From the results of these examples it appears that further study and calculations of cloud height and attenuation along these lines would be worth while. More TIROS data are now available.

6. CONCLUSION

In spite of the indirect method of obtaining the heights of cloud bases and tops, and in spite of the uncertainty in using air temperature in a cloud composed of liquid water droplets to obtain black body cloud flux, it appears that a preliminary climatology of the effective emissivity of clouds following this method is of value.

Moreover, the implications for cloud height determination as an adjunct to working out satellite cloud height techniques are of interest. Large changes in apparent earth temperature, measured by satellite sensors, may be quantitatively explained along lines such as those discussed and it is in these latter two lines of research that further work may be beneficial as a satellite backup study.

REFERENCES

1. A. W. Brewer and J. T. Houghton, "Some Measurements of the Flux of Infra-Red Radiation in the Atmosphere," *Proceedings of the Royal Society*, Series A, vol. 236, 1956, pp. 175–186.
2. R. H. Bushnell and V. E. Suomi, "Experimental Flight Verification of the Economical Net Radiometer," *Journal of Geophysical Research*, vol. 66, No. 9, Sept. 1961, pp. 2843–2848.
3. D. M. Gates and C. C. Shaw, "Infrared Transmission of Clouds," *Journal of the Optical Society of America*, vol. 50, No. 9, Sept. 1960, pp. 876–882.
4. J. L. Gergen, "Blackness of Clouds as Determined from Radiation Measurements," Technical Report, Atmospheric Physics Program, School of Physics, University of Minnesota, Dec. 1958, pp. 1–92.
5. J. L. Gergen, "Note on the Paper by Herbert Riehl, 'Radiation Measurements over the Caribbean During the Autumn of 1960,' " *Journal of Geophysical Research*, vol. 68, No. 7, Apr. 1, 1963, pp. 2063–2064.
6. P. M. Kuhn, "Accuracy of the Airborne Economical Radiometer," *Monthly Weather Review*, vol. 89, No. 8, Aug. 1961, pp. 285–287.
7. P. M. Kuhn, "Soundings of Observed and Computed Infrared Flux," *Journal of Geophysical Research*, vol. 68, No. 5, Mar. 1, 1963, pp. 1415–1420.
8. R. A. McGee, "An Analytical Infrared Radiation Model of the Earth," *Applied Optics*, vol. 1, No. 5, Sept. 1962, pp. 649–653.
9. H. Riehl, "Radiation Measurements over the Caribbean During the Autumn of 1960," *Journal of Geophysical Research*, vol. 67, No. 10, Sept. 1962, pp. 3935–3942.
10. S. D. Soules, personal communication with author, May 1962.
11. V. E. Suomi and P. M. Kuhn, "An Economical Net Radiometer," *Tellus*, vol. 10, No. 1, Feb. 1958, pp. 160–163.
12. D. Q. Wark, G. Yamamoto, and J. H. Lienesch, "Methods of Estimating Infrared Flux and Surface Temperature from Meteorological Satellites," *Journal of the Atmospheric Sciences*, vol. 19, No. 5, Sept. 1962, pp. 369–384.